ULTRASONIC MEASUREMENT OF THE RESIDUAL

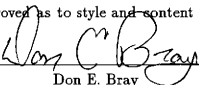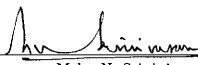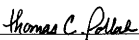# STRESSES IN PATCH WELDED STEEL PLATES

A Thesis

by

PAUL GERARD JUNGHANS

Submitted to Texas A&M University
in partial fulfillment of the requirements
for the degree of

MASTER OF SCIENCE

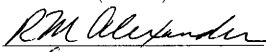Approved as to style and content by:

_____
Don E. Bray
(Chair of Committee)

_____
Thomas C Pollock
(Member)

_____
Malur N Srinivasan
(Member)

_____
for G. P. Peterson
(Head of Department)

May 1994

Major Subject: Mechanical Engineering

ABSTRACT

Ultrasonic Measurement of the Residual Stresses

in Patch Welded Steel Plates. (May 1994)

Paul Gerard Junghans, B.S., Texas A&M University

Chair of Advisory Committee: Dr. Don E. Bray

This study begins with a review of the nature and origins of residual stresses and the techniques currently used to measure these stresses, both destructive and nondestructive. The theory of ultrasonic stress measurement, acoustoelasticity, is discussed in detail, with special emphasis on the use of critically refracted longitudinal (L_{CR}) waves. The ultrasonic stress measurement technique used in this study utilizes L_{CR} waves that are transmitted and received on the same surface and travel just beneath the surface of the plate. The stresses within the plate affect the travel time of these waves in accordance with the acoustoelastic relationship

Considerable attention has been directed toward the use of high angle, longitudinal waves for both nondestructive inspection and stress evaluation. To further the understanding of the characteristics of these waves, longitudinal and shear wave beam profiles are presented for the L_{CR} wave transducer used in this study and for a commercial creeping wave transducer. The results show that both probes do indeed produce a critically refracted longitudinal wave as well as a trailing shear wave that is refracted into the material at a much lower angle, approximately 33°. Furthermore, the simple and accurate method developed to measure the radiation patterns from these transducers also is presented.

Differences in the ultrasonic travel times of the L_{CR} wave were obtained in a stress relieved and a non-stress relieved 13 mm (1/2 in.) thick, structural steel plates. The two 1.2 m (48 in.) square plates were patch welded in the center to create a residual stress field; and subsequently, one of the plates was stress relieved.

The L_{CR} travel-time measurements on the plates not only differentiated between the residual stress states but also gave some indication of their distribution and magnitude. Neither texture nor the localized residual stresses significantly affected the results. These findings verify that they L_{CR} ultrasonic technique can indeed measure weld induced residual stresses and demonstrate the potential of this technique for evaluating the state of post-weld heat treatment in common structural steel.

"It is true that nature begins by reasoning
and ends by experience Nevertheless, we must begin
with experiments and try through it to discover the reason."

– Leonardo da Vinci –

TABLE OF CONTENTS

LIST OF TABLES

LIST OF FIGURES

INTRODUCTION

Determining the magnitude and distribution of residual stresses within manufactured items has always been a major concern of engineers. The direct superposition of residual stresses onto applied stresses can be advantageous, as in pre-stressed concrete. However, when they are not properly accounted for, residual stresses can also prove disastrous, as in the spontaneous, catastrophic failure of the S.S. Schenectady[1] shown in Figure 1.
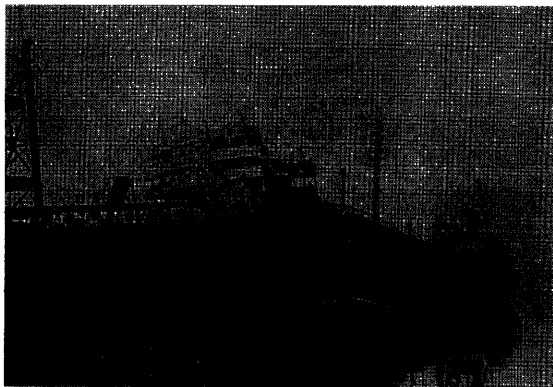
Fig 1   The catastrophic failure of the S.S. Schenectady in calm water was promoted by flaws and high residual stresses in the welds. Adapted from Nelson[1].

This thesis follows the style and format of *NDT International*.

The problem of measuring these 'hidden' stresses is usually difficult; and, current methods for measuring residual stresses are limited in their capabilities and often uncertain in their results[2]. In recent years, ultrasonic stress measurement techniques have generated a great deal of interest because of their distinct advantages. They are nondestructive, inexpensive, accurate, and relatively simple to use. Ultrasonic methods have shown great promise for accurately resolving the residual stress patterns in many different materials. Much work is still needed to refine these methods into systems that are easy to use, consistently accurate, and simple enough to be widely adopted. Reference standards suitable for refining and calibrating these residual stress measurement systems must also be developed. To date, commercial equipment specifically designed for ultrasonic stress measurement is not yet available but may be soon.

RESIDUAL STRESSES

The type of residual stresses examined in this study are often termed macro-residual stresses since their effects extend over relatively large regions as compared to microresidual stresses in metals which are frequently restricted within single grains of the material. Macroresidual stresses are analogous to common engineering stresses created by applied loads. In order to limit redundancy, the term residual stress shall henceforth imply macroresidual stress.

Residual stresses are present in most fabricated components because they are produced by nearly all manufacturing processes. Thermal gradients, plastic defor-mation, and reactions between components in an assembly can all create significant residual stresses. These hidden stresses usually give no outward indication of their presence and, yet, may be as high as the yield strength of the material

It is often difficult to conceptualize the residual stresses present in a component free of external loading. While the stresses created by applied loads in a item may be easily calculated, how can an engineer calculate or measure the residual stresses that may also be present? Since the residual stresses will add directly to any stresses in the component, an understanding of the distribution and magnitude of the residual stresses is just as important as an understanding of the applied loads when attempting to predict failure

Definition of Residual Stresses

Corresponding to any residual stress field is an internal distribution of strains. This internal residual strain field represents a storage of elastic energy within the material[3]. For isotropic elastic materials, the residual strain distribution at any

point, ϵ_i, can be calculated from the residual stress state at that point, σ_j, by using the generalized form of Hooke's Law·

$$\epsilon_x = \frac{1}{E}[\sigma_x - \nu(\sigma_y + \sigma_z)]$$

$$\epsilon_y = \frac{1}{E}[\sigma_y - \nu(\sigma_x + \sigma_z)] \qquad (1)$$

$$\epsilon_z = \frac{1}{E}[\sigma_z - \nu(\sigma_x + \sigma_y)]$$

where E is the Young's modulus of the material and ν is the Poisson's ratio. Below their yeild strength, most metals may be considered to be isotropic, elastic materials.

When considering residual stresses, two interesting points should be noted. The distribution of residual stresses within a component will always satisfy static equilibrium requirements through any complete cross section of the component. And, the magnitude of these stresses will always be less than or equal to the yield strength of the material. It is also noteworthy that the principal directions of residual stress fields are quite frequently aligned with the directions of primary interest, such as the rolling direction in sheets or radial and tangential directions in cylinders[3].

This brief summary on residual stresses will be quite helpful in understanding how these stresses are created within components and how the current measurement techniques function.

Effects of Residual Stresses

The effects that residual stresses will have on a component's performance are often difficult to predict but can be significant. The superposing of residual stresses on applied stress distributions is a useful and widely exploited effect Obviously, residual stresses that counter applied stresses can greatly improve a component's performance. For example, when residual compressive stresses are induced on a metal component's surface, as by shot-peening, its fatigue strength and stress-corrosion cracking resistance are improved; unfortunately, these surface compressive stresses

also reduce the yielding strength of the component. Residual stresses can be used to improve the inherent performance of many types of materials. When compressive residual stresses are induced in concrete, the ultimate tensile strength is increased; but, this is only by and with an equivalent reduction in its ultimate compressive strength. The beneficial and detrimental effects of residual stresses must be carefully balanced.

One of the most notorious effects of residual stresses is the dimensional instability which they cause. When material is machined away from a component containing residual stresses, the continuous redistribute of the stresses in order to maintain static equilibrium can produce significant distortion in the component.

Many other mechanical, electrical, magnetic, and chemical properties are influenced by residual stresses. However, these effects are essentially all consequences of the internal strain energy that residual stresses represent. Though subtle and elusive, residual stresses are nevertheless subject to analytical and experimental analysis. They obey the fundamental principles of physics and originate through mechanisms which we may reasonably expect to understand[3]. Reliable information and sound judgement, however, are required.

ORIGINS OF RESIDUAL STRESSES

Since almost every type of manufacturing process produces some sort of residual stress, it would be difficult and lengthy to explain the origins of residual stresses by relating them to the manufacturing processes by which they were produced. A simpler and more direct approach lies in categorizing residual stresses by the underlying physical phenomenon which produce the internal strain distribution. There are three distinct phenomena to which residual stresses can be attributed: non-uniform volume changes, non-uniform deformations, and assembly reaction stresses[3]. A brief discussion and example of each follows. It should be possible to classify all residual stresses into one of these categories, though the distinction may not always be perfectly clear.

Residual Stresses in a Weld Due to Non-uniform Volume Changes

A residual stress field is created whenever a non-uniform volume change occurs within a material. The most frequent and significant residual stresses from non-uniform volume changes are encountered in connection with the solidification and subsequent cooling of material from its liquid phase. This is because the corresponding phase transformation and thermal contraction of the liquid produces relatively large volume changes that rarely occur in a uniform manner. Other processes such as diffusion, precipitation growth, and solid–solid phase transformations can also produce significant non-uniform volume changes which create residual stresses.

An analysis of the welding process provides an excellent example of how non-uniform volume changes produce residual stresses. Complex interactions between solidification, thermal expansion, contraction, and plastic yielding produce high
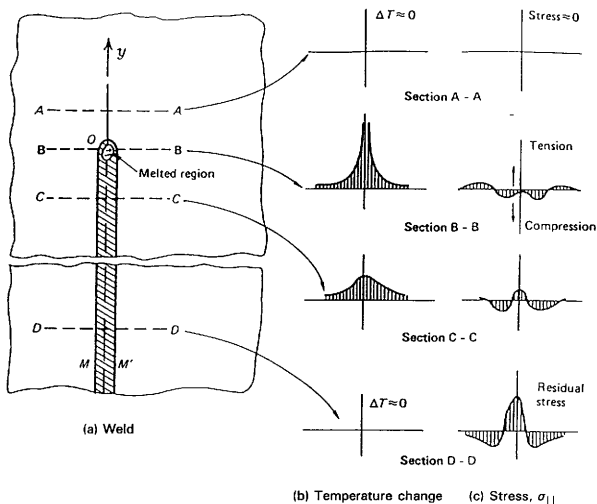
Fig. 2. Schematic representation of the changes in temperature and tangential stress, $\sigma_\parallel$, during the welding process moving in the Y direction. Adapted from Mordfin[4]

residual stresses in welds. Figure 2 provides a schematic representation of the changes in temperature and stress during the welding process[4].

The distribution of tangential stresses, ie. stresses oriented parallel to the weld, shall be considered since they are of the highest magnitude. The plate is assumed to be at a uniform temperature and free of both applied and residual stresses before the welding occurs, as represented by section A–A. At the weld arc, section B–B, the temperature of the plate is equal to the melting point of the weld material; and, the

stresses in the molten metal are equal to zero since an unconstrained fluid cannot support a load. The material directly adjacent to the melted region expands due to high temperature. This expansion is restrained by the surrounding cooler material; thus, compressive thermal stresses are created near the weld arc. These are statically balanced by tensile stresses in the surrounding cooler material. Behind the weld arc, the material solidifies quickly and begins to cool. As shown in section C–C, the thermal contraction of the cooling weld creates tensile stresses at and adjacent to the weld. The weld, which was long enough while hot, is now strained elastically and often plastically to fill the entire length of the cooler weld channel. Compressive stresses are established in the surrounding material thus static equilibrium is maintained. The tangential tensile stress at the weld may be as high as the yield strength of the material. The typical residual stress distribution for a weld at thermal equilibrium is shown in section D-D.

Even though other factors, such as solid–solid phase transformations and thermal gradients through the thickness are involved, the final residual stress distribution in a weld is almost completely determined by the liquid–solid phase transformation and subsequent thermal contraction. It should also be noted that the stress distribution shown in Figure 2 is incomplete. In reality, a biaxial state of residual stress actually exists in all welded plates[5], as shown in Figure 3. The residual stress state of a welded plate is characterized by both a tangential stress distribution as well as a transverse stress distribution, i.e. oriented perpendicular to the weld[6].

Residual Stresses Due to Non-uniform Deformations

With the exception of parts which are cast into their final shape, most metal components are fabricated by manufacturing processes which involve plastic deformation, and, these deformation processes are seldom uniform[3]. Any operation which produces a non-uniform plastic deformation in a metal component will inevitably generate residual stresses. Thus, it may be concluded that residual stresses are present
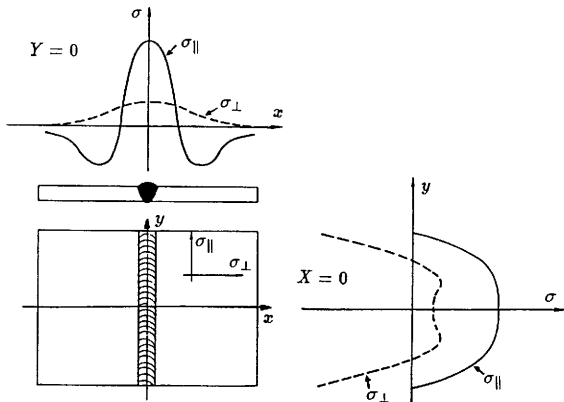
Fig 3. Biaxial residual stress distribution in planes perpendicular (above) and parallel (right) to a weld where $\sigma_{\parallel}$ and $\sigma_{\perp}$ represent the tangential and transverse stresses, respectively. Adapted from Wohlfahrt[5].

in nearly all manufactured items Rolling, drawing, stamping, pressing, bending and even machining all produce non-uniform deformations within the work-piece. Most common manufacturing processes produce a complex distribution of residual stresses that directly opposes the non-uniform deformation that has occurred in the material.

Consider the simple example a bent steel bar, as shown in Figure 4. If small bending moments are applied, a linear elastic stress distribution is created within the beam that is equal and opposite to the applied moments The stress is zero at the center of the beam, the neutral axis, and varies linearly to the maximum tensile and compressive stresses at the upper and lower surfaces, respectfully. If the beam is unloaded at this point, it will spring back to its original stress-free shape since no

(a) Elastic Stress Distribution

(b) Elastic\Plastic Stress Distribution

(c) Residual Stress Distribution
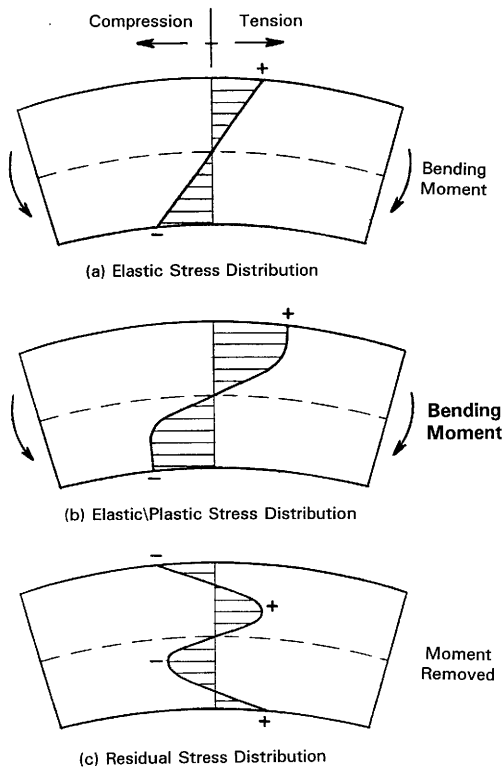
Fig. 4. The distribution of stresses within a steel bar during and after bending.

permanent plastic deformation has occurred. If larger bending moments are applied on the beam, the stresses at the upper and lower surfaces will eventually reach the yield strength of the material and plastic deformation will occur. With yielding, an elastic and plastic stress distribution is created within the beam. The stress at the neutral axis remains zero; but, the stress distribution is longer linear. The stresses rise to a plateau near the outer surfaces at a value equal to the yielding strength of the material. If the loading is increased further, the plastic yielding zones will extend inward and the stress gradient at the center will increase. When the load is removed after yielding, the stress within the beam does not return to zero. A residual stress distribution is created by non-uniform plastically deformation. The outer surfaces have been strained beyond their elastic limit. As the elastic strain in the center of beam springs back, compressive and tensile stresses are created at the upper and lower surfaces, respectively. The stresses in the yielded portion of the beam are balanced by stresses in the non-deformed material at the center of beam, in such a way, that the distribution satisfies the static equilibrium requirement.

Residual Stresses Due to Assembly Reactions

The reactions between the components of an assembly will create stresses within the components even when no external loads are applied to the assembly. The reaction forces created by interference fits, mis-alignments in construction, and even the weight of the components themselves can produce significant residual stresses. Sometimes referred to as 'reaction stresses'[3] or 'mechanical residual stresses'[7], these types of stresses are often not considered to be true residual stresses because of their unique nature Since they are created by the interactions between components, assembly reaction stresses can be calculated with standard engineering formulas and can often be measured with applied stress measurement techniques, such as strain gages. If gages are mounted and balanced before the assembly is constructed, the strain produced by the interactions between the components can be measured; and, the

reaction stresses that are produced in the assembly can be calculated. These unique features of assembly reaction stresses can be exploited in the development of the residual stress calibration standard.

Pre-stressed concrete is an excellent example of how assembly reactions can be used to create beneficial residual stresses. After a concrete slab has hardened, the steel reinforcement bars, which are embedded within it, are elastically strained in tension by hydraulic jacks and capped with steel plates at the edges of the concrete. The reaction forces created by the tension in the reinforcement bars are balanced by a compressive stresses within the concrete. Thus, the ultimate tensile strength of the concrete is improved through the intentional use of assembly reaction stresses.

RESIDUAL STRESS MEASUREMENT TECHNIQUES

Many excellent techniques already exist to determine the stresses in a component created by applied loads. These include electrical resistance gages, brittle coatings, moiré-fringe analysis, finite element modeling and photoelasticity. These are all very useful tools to measure and/or predict the distribution of applied stresses within a part. Unfortunately, these methods can not be used to determine the distribution of residual stresses that may also be present in the component.

Many techniques have been proposed to solve the problem of residual stress measurement. The commonly used destructive methods for measuring residual stresses are dissectioning, hole drilling and hydrogen-induced cracking. Since the stress distribution obtained by these techniques apply to the parts which have been destroyed or damaged in the process, the true distribution of stresses within the in-service parts is only inferred. Virtually all of the physical phenomena used for nondestructive evaluation have been evaluated for a capability to measure residual stresses. Several nondestructive methods, such as diffraction, barkhausen noise, and acoustoelasticity, are currently being developed and used to measure residual stresses. These are indirect measurement techniques and are often limited by metallurgical and geometric factors. Each of these methods has distinct advantages and limitations; thus, none has yet proven to be the universal or preferred solution.

It is useful to briefly review the commonly used residual stress measurement techniques in order to compare their capabilities and emphasize the unique character of the L_{CR} ultrasonic technique that is used in this study. More extensive reviews of these techniques are available in the literature, see Mordfin[2] and Treuting et al[3].

Destructive Techniques

Dissectioning is one of the time-honored methods of residual stress measurement. When components are dissectioned into layers, the deformation in each layer can be used to determine the residual stress distribution throughout the body. As each layer is cut away, a redistribution of the internal strains occurs to maintain static equilibrium. The resulting deformation, created by this redistribution, can be measured and used to calculate the stresses within the part.

Dissectioning, though straightforward and reasonably accurate, is fairly difficult and time consuming in practice. Furthermore, this technique only approximates the stress distribution from the stresses within each of the layers sampled throughout the volume of the part   Greater confidence and accuracy can only be obtained by the intricate testing of several identical parts. This method is best suited for settings where large numbers of parts are manufactured by well-controlled, repeatable processes.

Hole Drilling or **Blind-Hole Drilling**, as it is sometimes called, is another widely used technique for residual stress measurement. This method requires that a rosette strain gage be mounted at the desired measurement point. A rigidly-guided mill is used to drill a hole directly in the center of the three elements of the rosette gage. The residual stresses are calculated from the strains created by the surface relaxation caused by the removed material. This technique is sometimes considered only semi-destructive because the drilled hole is relatively small, usually 1.5 mm to 3.0 mm (.06 to .12 in.) in both depth and diameter; and, the part can sometimes be returned to service.

Attributes of the blind-hole drilling technique include the fact that it is experimentally and analytically simple and that the required equipment is fairly inexpensive and commercially available However, hole drilling is semi-destructive at best, limited to flat surfaces, and provides information on only the near-surface stress distribution.

The **Hydrogen-Induced Cracking** technique can be used to qualitatively evaluate the residual stress distribution in certain types of steels. When a steel part is exposed to hydrogen gas or a dilute aqueous solution, hydrogen embrittlement cracking will occur in areas of high tensile stress. Thus, a visual or penetrant inspection of the part will reveal pattern of cracks that is perpendicular to the surface distribution of tensile residual stresses. This technique is limited to materials that are suseptible to hydrogen embrittlement; and, it destroys the part that is tested.

Nondestructive Techniques

X-ray Diffraction is the most widely used technique for measuring residual stresses[8]. This technique is based upon the relationship between surface stresses in a crystalline material and the angle of X-ray diffraction. It is known that stress alters the interplanar lattice spacing in crystalline materials. Since the angle of X-ray diffraction is dependent on this spacing, the stress levels in crystalline materials can be correlated to the angle at which the surface diffracts X-rays. A major limitation of this method is the depth of investigation which is limited to only about 0025 mm (.0001 in.) since X-rays are highly attenuated in steel[3].

The X-ray diffraction technique requires a fair amount of expertise in the preparation of the specimen and in the use of the equipment. X-ray equipment has historically been very expensive and too large to be portable; but, advances in electronics have reduced both the cost and size of the equipment. This method is limited to surface stresses in crystalline materials and conditions, such as material texture and surface finish, often produce significant errors. But even with these inherent limitations, X-ray diffraction is still one of the most universally accepted residual stress measurement techniques.

Neutron Diffraction can also be used to measure the lattice spacing in a crystalline materials; and thus, like X-ray diffraction, it can be used to calculate

residual stresses. An advantage of the neutron diffraction technique is that much deeper residual stresses can be sampled since neutrons can penetrate much further than X-rays. Unfortunately, a major limitation is the requirement of a high-flux neutron source, such as a nuclear reactor.

Barkhausen Noise refers to the acoustic emissions that occur in ferromagnetic materials during the alignment and subsequent relaxation of magnetic domains. When a ferromagnetic material is placed in a magnetic field, it becomes magnetized in a series of small, discontinuous steps which are attributed to the reorientation of individual magnetic domains. Whatever the cause, it has been observed that Barkhausen noise is affected by stress. It has been theorized that the residual stresses pin the electron domains thus changing the materials ferromagnetic response. Barkhausen noise has been used for a number of years to indirectly measure residual stresses; and, portable instrumentation is commercially available.

Application of the Barkhausen noise technique is limited to ferromagnetic materials and near-surface stresses. As with other nondestructive techniques, metallurgical factors such as grain size, texture, and strain hardening can have a significant effect on accuracy of this measurement. It should also be noted that the results are not always repeatable and that the incomplete understanding of the theoretical relationship between Barkhuesen noise and residual stress has somewhat limited its acceptance.

Ultrasonic stress measurement techniques, that are based upon the acoustoelastic relationship, are reviewed in the next two sections. The later section reviews the L_{CR} ultrasonic technique that is used in the patch weld stress measurement portion this study.

ULTRASONIC STRESS MEASUREMENT

Ultrasonic stress measurement techniques may ultimately emerge as the dominant nondestructive, residual stress measurement method for a variety of reasons. Ultrasonic techniques are capable of measuring both bulk and near-surface stresses since acoustic waves that propagate within the stressed material are utilized. Because these ultrasonic waves contain very little energy, a nondestructive inspection of the suspect component is possible. And, the underlying analytical theory as well as the acquisition and analysis of data are well understood and fairly simple.

The equipment required for ultrasonic stress measurement can be portable and is relatively inexpensive as compared to other methods. This acoustic acquisition equipment must be capable of highly accurate travel-time measurements since precision on the order of 0.025 μs or higher is usually required. The current state of electronic technology has greatly improved the availability and cost of such equipment. Suitable systems are available as expansion boards for personal computers, and, the data storage and analysis capablity which is needed for ultrasonic stress measurement also is now standard in most protable computers. Ultrasonic equipment specifically designed for stress measurement is not yet commercially available but recent developments suggest that this may not be far off[2].

Acoustoelasticity

All ultrasonic stress measurement techniques are based on acoustoelasticity, i e the hypothesis that there is a linear relationship between the acoustic wave speed and the elastic strain in the material. Acoustoelasticity and ultrasonic stress measurement are so innately related that the terminology used in the available literature fluctuates between these terms. The acoustoelastic effect on ultrasonic velocities is relatively small, on the order of a few hundreds of a percent[9]; and yet, it has been

used successfully for many years to measure bulk and near-surface stresses. In certain alloys, it has been suggested that this linear relationship between acoustic velocity and strain persists even beyond the yielding point in the material[10]. Allen *et al*[11] and Pao *et al*[12] have compiled excellent overviews of research on acoustoelasticity and ultrasonic stress measurement Specific examples of acoustoelastic stress measurement are too numerous to reference but are almost exclusively restricted to the simple case of uniaxial stress fields.

In a uniaxial stress field, there are five distinct combinations of wave type, propagation direction, and wave polarization, as shown in Figure 5. For the sake of clarity, a double subscript notation is henceforth adopted to distinguish the five unique combinations. The first subscript refers to the direction of wave propagation, and the second subscript refers to the direction of wave polarization, i e. particle motion.

Two of the five distinct wave combinations are longitudinal (dilatational) and three are shear (torsional). When the applied stress is assumed to be in direction 1, the V_{11} wave is a longitudinal wave propagating in the direction of the applied stress. This wave combination exhibits the largest acoustoelastic effect and is the type used for the L_{CR} ultrasonic stress measurement technique. The V_{12} wave is a shear wave, i e. polarized perpendicular, propagating parallel to the applied stress. The V_{22} wave is a longitudinal wave propagating perpendicular to the applied uniaxial stress field. The V_{23} wave is a shear wave that is polarized and propagating perpendicular to the applied stress Finally, the V_{21} wave is a shear wave that is polarized parallel to the applied stress but propagating perpendicular to it. All of these acoustoelastic wave combinations, with the possible exception of the V_{22} wave, have been exploited at one time or another for ultrasonic stress measurement.

Egle and Bray[13] measured the strain-induced changes in the wave velocities of common rail steel for each of the five wave combinations. The results, shown in Figure 6, indicate that the acoustoelastic effect is indeed linear in the elastic range, as theory predicts, and of sufficient magnitude to be used for stress measurement. Theoretical expressions for the acoustoelastic effect have been derived by Hughes and
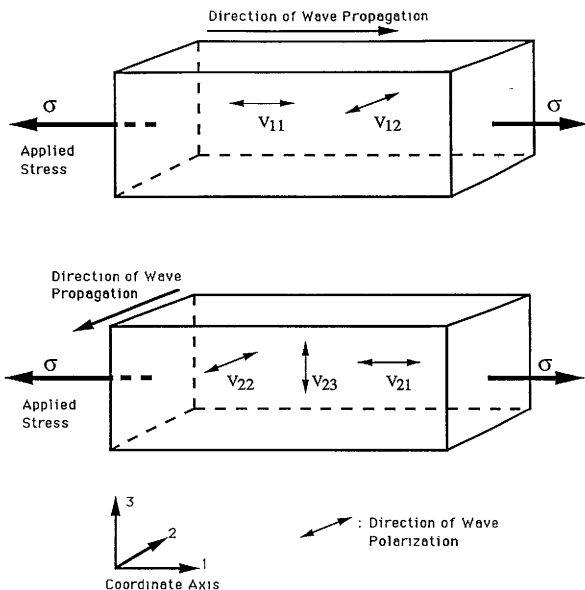
Fig. 5.   The five distinct acoustoelastic wave combinations in a uniaxial stress field. The double subscript refers to the direction of wave propagation and wave polarization, i.e. particle motion, respectively.
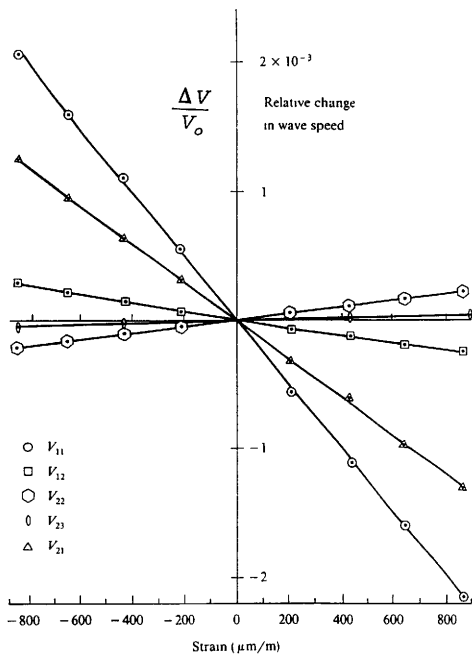
Fig. 6. Relative changes in the wave velocity as a function of axial strain for rail steel. Adapted from Egle *et al*[13].

Kelly[14] Furthermore, the results show that each of the five wave combinations has a distinct acoustoelastic constant, i.e. slope. The largest effect is associated with a longitudinal wave propagating parallel to the applied stress, the V_{11} wave. Egle and Bray[13] noted in their work that "... the agreement with values found by other investigators for other steels suggests that the acoustoelastic constants, as well as the third–order constants, may be relatively independent of the specific composition and heat treatment as is the case for the second–order constants." If true, the consequence of this relative independence on the development of residual stress measurement is far reaching and significant.

Consideration of the Ultrasonic Stress Measurements Parameters

Material texture and temperature can produce significant variations in ultrasonic wave speeds as compared with the relatively small acoustoelastic effect. The difficulty in differentiating the velocity changes associated with stress from those associated with texture has been a major restriction in the development of acoustoelastic stress measurement systems. The effect of material texture is difficult to predict; and, current methods for measuring and correcting for texture are unreliable. The linear effect of temperature on ultrasonic wave speeds is much easier to compensate since the temperature of a specimen can be accurately and repeatedly determined.

Bray and Leon-Salamanca[15] proposed a useful model of the parameters that affect ultrasonic velocities when they presented their method for obtaining zero-force travel-times. If we consider a material under load, the ultrasonic velocity within the material is altered by the combined effects of the applied forces, residual stresses, material texture, and the ambient temperature. This can be expressed by:

$$V = V^* + \Delta V_F + \Delta V_{RS} + \Delta V_{TX} + \Delta V_T \tag{2}$$

where

V – measured velocity,

V^* – velocity for a homogenous, isotropic, stress-free material at a standard temperature,

ΔV_F – velocity change due to applied forces,

ΔV_{RS} – velocity change due to residual stresses,

ΔV_{TX} – velocity change due to material texture, and

ΔV_T – velocity change due to deference in temperature from the standard.

For ultrasonic stress measurement, ΔV_F and ΔV_{RS} are the parameters of interest; but, V is the parameter which is actually measured. Consequently, a scheme must be devised to calculate or measure the effects of the other parameters, either individually or collectively.

The separation of the effect of the residual stresses from the effect of the applied forces is very difficult since both affect the wave speed in a similar manner. But is this separation really necessary? In many cases it is not, since the total stress level is of interest. In many other cases, the applied forces may be known and, therefore, removed so that the effects of the residual stresses are isolated

The linear relationship of temperature and ultrasonic wave velocities is well documented. Egle and Bray[16] determined the effect of temperature on the velocity of longitudinal and shear waves in pearlitic steel to be $0.55 \frac{m}{s\,^\circ C}$ and $-0.38 \frac{m}{s\,^\circ C}$, respectively. With values such as these, the effect that ambient temperature has on experimental velocity measurements, ΔV_T, can easily be corrected to a convenient standard reference temperature.

The term texture refers to a material's anisotropic microstructure. Texture in metals may result from directional solidification or mechanical cold working during fabrication. Whatever the cause, the fact that the grains in a polycrystalline materials can exhibit a preferred orientation creates a serious problem in ultrasonic stress measurement. Material texture can produce relatively large changes in the velocities of ultrasonic waves. Musgrave[17] reported a considerable variation in longitudinal wave speed as a function of direction in a single crystal of steel, as much as 18%. This variation in wave speed with respect to crystalline direction indicates that any non-random distribution of microstructure will result in texture-induced anisotropy

of the material's ultrasonic velocity. Although in most polycrystalline materials, such as structural steel, the degree of preferred orientation is unlikely to exceed even a few percent[11], the effect created by even this level of texture can be on the order of 10^{-2}; whereas, the comparable effect due to stress may only be on the order of 10^{-4}.

Several methods have been proposed to separate the velocity changes associated with texture from those associated with stress. One solution is to have a stress free reference sample that is identical to the stressed component in every way, including texture. Thus, any differences in the ultrasonic velocities in the two parts would be solely due to stress. However, the problem of confirming the textural equivalence of the two parts is somewhat difficult. Another solution exists for materials that can be assumed to have constant texture, such as rolled sheets. The variations in ultrasonic wave speeds in a given direction in such materials should be directly proportional to stress since there would be no variation due to texture. Other methods have been proposed including texture independent combinations of ultrasonic velocities[9] and frequency analysis of the acoustic birefringence waves to measure texture-induced anisotropy[18]. Though all of these methods are useful, a universal solution to the problem of texture for ultrasonic stress measurement has not yet emerged.

For the measurement of residual stresses, a stress free reference velocity is required for comparison. This reference velocity is equal to the stress free velocity of the material plus any adjustments required for ambient temperature and texture of the particular specimen:

$$V_o = V^* + \Delta V_T + \Delta V_{TX} \qquad (3)$$

where V_o is the stress free reference velocity. This reference velocity may be obtained from measurements on a stress free sample of the material that is known to have equivalent texture or by measurements in a stress free portion of the actual specimen. If the specimen under examination is free of applied forces ($\Delta V_F = 0$), the change in the ultrasonic velocity due to the residual stress may be expressed as:

$$\Delta V_{RS} = V - V_o \qquad (4)$$

which is obtained by combining Equations 2 and 3. The ramifications of this equation are obvious. The effect of residual stress on velocity of ultrasonic waves has been isolated. By using this expression along with the appropriate acoustoelastic constants, residual stresses may be calculated from experimentally measured ultrasonic velocities.

Acoustic Birefringence Technique

Acoustic birefringence is probably the most well documented ultrasonic stress measurement technique. Shear wave birefringence, as it is sometimes called, is analogous in many ways to the phenomenon of optical birefringence in photoelastic materials. As previously noted, the velocity of ultrasonic shear waves in a stressed material are not only dependent on the direction of propagation but also on the direction of wave polarization. The acoustic birefringence technique utilizes two shear waves propagating perpendicular to the stress field. One shear wave is polarized parallel to the direction of the stress while the other shear wave is polarized perpendicular As previously termed, these are the V_{21} and V_{23} waves, respectively. The V_{21} wave demonstrates a significant effect from applied or residual stress whereas the V_{23} wave is relatively unaffected. The stress within a specimen is calculated from the difference of the relative velocities of these two waves.

Problems with the acoustic birefringence technique arise from the requirements for a fully isotropic material as well as a clearly defined travel path from which the ultrasonic velocities can be measured. Anisotropy due to material texture causes significant changes in the relative shear wave speeds. Often being several orders of magnitude greater than the effect of stress, these texture-induced changes are the single greatest hindrance to the acoustic birefringence technique. Beam deviations from the expected travel path can also create apparent shifts in the velocity and lead to erroneous results.

THE L_{CR} ULTRASONIC TECHNIQUE

As research on the nondestructive measurement of stress has evolved over the years, it has become clear that the critically refracted longitudinal (L_{CR}) wave technique used at Texas A&M University offers some distinct advantages over the acoustic birefringence and other previously discussed techniques. The L_{CR} Ultrasonic Technique utilizes a high frequency acoustic wave which travels just below the surface of the material. Since this acoustic wave is a bulk wave, this technique is sensitive to the stress field in a finite thickness of the material and not just at the surface. A schematic of the L_{CR} wave is shown in Figure 7. Since the acoustic wave is generated and received from the same surface, beam deviations from the expected travel path are not likely. Therefore, travel time measurements obtained with the L_{CR} wave are not affected by reflections from the opposite surface. The results thus yield the true velocity of the material.
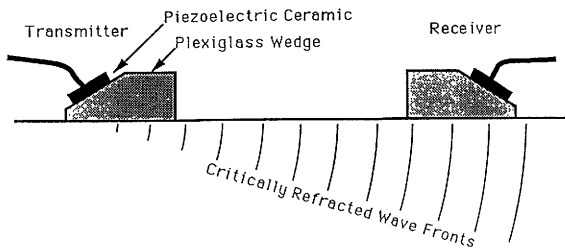
Fig 7. Schematic representation of a L_{CR} wave transmitter and receiver as well as the generated wave fronts.

Another important advantage of the L_{CR} ultrasonic technique is its stress sensitivity. As previously show, the longitudinal wave propagating parallel to the stress field exhibits the largest acoustoelastic effect. The L_{CR} ultrasonic technique utilizes this wave combination, previously denoted as the V_{11} wave. Thus, for an given data acquisition system, the L_{CR} technique will produce a most precise acoustoelastic stress measurement. In comparison to the shear waves used for acoustic birefringence, the longitudinal waves are more sensitive to stress and yet are less sensitive to material texture[15,19]. This characteristic minimizes the effect of material texture on the accuracy of the stress measurement.

In the case of uniaxial stress where the effects of temperature and texture may be included in the reference velocity, the change in stress from the stress free reference level is calculated directly from the change in the V_{11} wave velocity[15] by:

$$\Delta\sigma = \frac{E}{A_{11} * V_o}(V - V_o) \tag{5}$$

where

$\Delta\sigma$ – change in stress from the reference level at which V_o was measured,

E – Young's modulus of the test material,

V_o – stress-free reference velocity,

A_{11} – appropriate acoustoelastic constant, and

$(V - V_o)$ – change in velocity due to stress.

This relationship may also be expressed in terms of travel times rather than the velocity if the measurement distance, i.e. the L_{CR} probe length, is factored out of the expression.

The significant problem with the L_{CR} ultrasonic technique has historically been the length of the probe. Much of the L_{CR} stress measurement research was conducted with probes that were constructed with three transducers, one transmitter and two receivers[20,21]. The three-transducer design was originally adopted since a pulse overlay measurement technique was needed to obtain the required travel-time accuracy[20]. This type of design produces a lengthy probe, often as long as 48 cm (19 in). The length of the L_{CR} probes made acoustic coupling difficult and limited

the applicability of this technique to large specimens such as railroad rails or large plates. With the advent of very high speed digital oscilloscopes, the pulse overlay or sing-around techniques are no longer needed to obtain the required accuracy. A new probe design that is currently being developed at Texas A&M University utilizes a transmitter and a single receiver. An innovation of this new design is that the transducer spacing is easily adjustable. It is hoped that this design will greatly reduce the problems associated with coupling and length while preserving the unique advantages of the L_{CR} ultrasonic technique.

Characteristics and Excitation of the L_{CR} Wave

As previously noted, the L_{CR} wave is a bulk longitudinal wave traveling just below the surface of the specimen. This type of wave is analogous to a compressional head wave in seismology.

The L_{CR} wave has several interesting and useful characteristics. Since it is a critically refracted longitudinal wave, it is the fastest wave and is traveling along the shortest possible path. Therefore, the L_{CR} wave is easy to distinguish since it is always the first arrival at the receiver. A typical oscilloscope trace of an undamped L_{CR} wave arrival is shown in Figure 8. The waves direct arrival, clean signal, and temporal isolation from other wave modes allows the precision in travel-time measurements to be significantly less than a single wavelength. Another useful characteristic is that the L_{CR} wave is relatively insensitive to surface roughness and geometry[22,23]. Thus, the surface condition of the specimen has little effect on L_{CR} stress measurements.

In this study, the L_{CR} wave was excited with a transducer specifically designed to produce a critically refracted longitudinal wave in structural steel plate. A schematic of the L_{CR} wave transducer is shown in Figure 9. A planar longitudinal wave is generated in a Plexiglas wedge by a piezoelectric plate which is epoxied onto the angled surface. The piezoelectric plate, made of a PZT ceramic, is 2.54 cm (1.0 in) square and has a nominal resonant frequency of 2.25 MHz in the thickness mode.
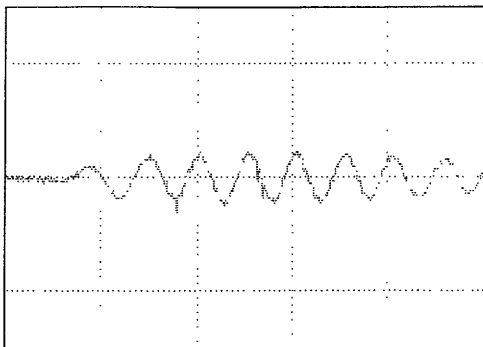
Fig. 8. Digital oscilloscope trace of a 2.25 MHz L_{CR} wave arrival.

The longitudinal wave is generated at the first critically angle of refraction. The first critical angle of refraction refers to the angle at which a longitudinal wave is generated along the surface of the test specimen, i.e. at 90°. If the angle of incidence is less than this critical angle, the principle longitudinal wave is refracted into the test specimen at some angle less than 90°. If the angle is significantly greater than critical angle, most of the longitudinal energy is reflected at the transducer/specimen interface and essentially no longitudinal wave is generated within the test specimen. Refraction of the incident longitudinal wave at the transducer/specimen interface not only excites a refracted longitudinal wave but also the slower, mode converted shear
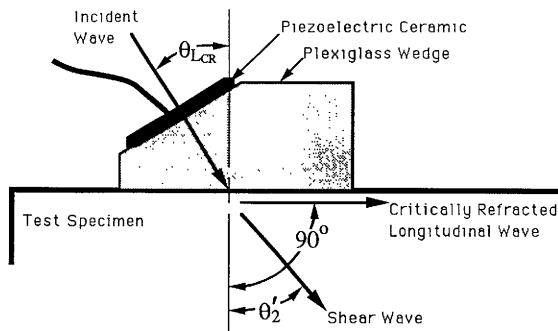
Fig 9   Schematic of the L_{CR} wave transducer showing ray paths.

wave at a lower trailing angle, C_2'.

In the previous discussion, the wave speed in the test specimen is different than that in the wedge material and the refraction at the interface occurs in accordance with Snell's Law:

$$\frac{sin\theta_1}{C_1} = \frac{sin\theta_1'}{C_1'} = \frac{sin\theta_2'}{C_2'}$$ (6)

where

   θ_1 − angle of the incident wave,

   C_1 − longitudinal wave speed in the wedge,

   θ_1' − angle of refracted longitudinal wave,

   C_1' − longitudinal wave speed in the test specimen,

   θ_2' − angle of refracted shear wave, and

   C_2' − shear wave speed in the test specimen.

For the special case of the L_{CR} wave ($\theta'_1 = 90°$), Equation 6 may be solved for the first critical angle of refraction, $\theta_{L_{CR}}$:

$$\theta_{L_{CR}} = \theta_1 = sin^{-1}(\frac{C_1}{C'_1}) \qquad (7)$$

The first critical angle for a longitudinal wave at a Plexiglas/steel interface[24,25] is approximately equal to 27°30′ The exact value of the first critical angle is dependent on the longitudinal wave speeds in the wedge material and steel actually used; however, slight variations from this source rarely produce a significant effect. An error in the first critical angle of ±30′ does not lead to any appreciable change in radiated amplitude or reception sensitivity[22].

The generation of the L_{CR} wave is further complicated by the excitation of a trailing shear wave. If the L_{CR} wave is excited by an incident longitudinal wave at the first critical angle, the angle of the mode converted shear wave, θ'_2, can be determined from the relative longitudinal and shear wave speeds in the test specimen. Again, Equation 6 may be solved for this angle:

$$\theta'_2 = sin^{-1}(\frac{C'_2}{C'_1}) \qquad (8)$$

Since bulk shear waves travel at speeds about one-half to two-thirds the speed of longitudinal waves[25], the angle of refraction of the shear wave lags considerably behind the longitudinal wave. For a L_{CR} wave in steel, the shear wave angle, θ'_2, is approximately 33°. Trailing by both speed and travel path length, these waves are of no real consequence to the L_{CR} ultrasonic stress measurement technique.

The equations for the excitation of the L_{CR} wave have been developed in a general form as to be universally applicable. A more thorough discussion of the characteristics and excitation of L_{CR} waves is available in references [24], [26] and [27]. For further clarification of the L_{CR} probe's characteristics, the beam profiles of the L_{CR} wave transducer used in this study and a commercial creeping wave transducer are presented in the next section.

BEAM PROFILES OF TWO L_{CR} WAVE TRANSDUCERS

High angle, longitudinal wave transducers are required to generate and receive L_{CR} waves. This type of transducer has been designed and built at Texas A&M University for a number of years. The design is based upon acoustic wave theory, such as Snell's Law, as well as published research on the excitation of L_{CR} waves[22–27]. These transducers have produced excellent and repeatable results which correlate very closely with elastic wave propagation theory.

A knowledge of a transducers beam profile is essential whether one wishes to ultrasonically measure stress or nondestructively inspect a component. The beam profiles presented in this chapter demonstrate conclusively that the L_{CR} transducers made at Texas A&M do indeed produce critically refracted longitudinal waves and are well suited for acoustoelastic stress measurement. The beam profiles of a commercial creeping wave transducer are also presented for a comparison and evaluated for the possible application to L_{CR} stress measurement. Furthermore, this chapter presents the simple and accurate method which was developed to measure the refracted radiation patterns that the ultrasonic transducers produce in a test material[28].

Beam Profiling Test Plate

The beam profiling apparatus, shown in Figure 10, was designed to measure the radiation pattern that an ultrasonic transducer produces in a common structural steel. A 19.05 mm (.75 in.) thick steel plate was machined into a semi-circular shape with one end of the diameter flared. The radius of the plate was 7.1 cm (2.8 in.); and, it was constructed from a hot-rolled ASTM A-516, Grade 70 Steel This material exhibits longitudinal and shear wave speeds typical for a structural steel, 5810 $\frac{m}{s}$ (229,000 $\frac{in.}{s}$) and 3210 $\frac{m}{s}$ (126,000 $\frac{in.}{s}$),respectively. A hot-rolled steel plate

a) Photograph.
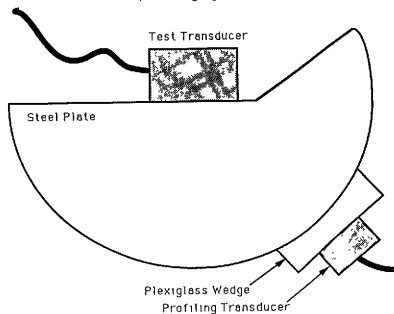
b) Schematic.

Fig. 10. A photograph and schematic of the beam profiling apparatus developed at Texas A&M University. Not shown to scale.

was selected to minimize the effect of the microstructural texture on the attenuation and wave velocities. This plate is of the type typically used in welded construction.

The special shape of the steel plate allows the test transducer to be positioned at the center of the arc so that the attenuation of the transducer's signal in the material is a constant at any point along the arc. The beam profile of the transducer is determined by measuring the strength of the ultrasonic signal along the arc with a profiling transducer. The profiling transducer is coupled to the arc of the steel plate with a curved Plexiglas wedge. The pie-slice addition to the half-circular shape allows the profiling transducer to remain completely coupled up to and even beyond a 90° refraction angle. Either a longitudinal or shear wave receiver may be used as the profiling transducer; thus, both wave modes may be profiled with the same test apparatus.

Since the signal's attenuation in the material is a constant, variations in the strength of the transducer signal are a direct result of both the transducer's refracted radiation pattern and the acoustic coupling of the profiling receivers. In practice, the strength of the ultrasonic signal is quantified as the amplitude of the profiling transducer's signal on an oscilloscope. The variations in the signal strength due to changes in the acoustical/mechanical coupling of the profiling transducer may be significant; however, these variations are random and can be reduced to a negligibly small level by averaging multiple trials. When multiple trials are averaged, the variations in the ultrasonic signal are directly proportional to the transducer's beam profile in the test material.

Experimental Design

The refracted radiation patterns of a L_{CR} wave transducer and of a commercial creeping wave transducer were measured with the beam profiling apparatus. The L_{CR} wave transducer was constructed at Texas A&M University It is designed to produce a strong, critically refracted longitudinal wave within a steel plate that can

travel a considerable distance parallel to the surface. The creeping wave transducer was a dual-element focused transducer, Model 83-613, made by Röntgen Technische Dienst, BV. It is the commercially available transducer that is most similar to the L_{CR} wave transducers made at Texas A&M. Both transducers have a nominal resonant frequency of 2.25 MHz.

The beam profiles of the transducers' longitudinal and shear wave signals in the steel plate were measured at 2.5° intervals from a 0° to a 90° angle of refraction Three complete and independent trials were performed on each transducer. These multiple trials reduced the effect of the random variations in the acoustic coupling of the profiling transducers Panametrics longitudinal and shear wave transducers, Model A1029 and V147, were used as the profiling transducers. These transducers also have a nominal resonant frequency of 2.25 MHz and are 13 mm (0.5 in.) in diameter. The strength of the profiling transducer's received signal was quantified as the maximum amplitude of the first arrival trace as displayed by an Epoch 2002 Ultrasonic Flaw Detector. The amplitudes of the received signals were standardized as a percentage of the maximum received signal from each trail. A complete listing of test data is presented in Appendix A.

Beam Profiles of the L_{CR} Wave Transducer

The longitudinal and shear wave profiles of the L_{CR} wave transducer were measured with the beam profiling apparatus The L_{CR} wave transducer is of the type used in the stress measurement portion of this study. It is design to produce a 2.25 MHz longitudinal wave in a Plexiglas wedge at an incident angle of 30° with respect to the steel test specimen. This angle is approximately 1° greater than the calculated first critical angle of refraction in the test material and is chosen to acheive maximum performance At this angle, some portion of the incident ultrasonic energy is reflected at the interface and remains within the transducer

The longitudinal and shear wave profiles of the L_{CR} wave transducer are plotted as a function of the refraction angle in Figure 11. The longitudinal wave profile shows that a L_{CR} wave is indeed generated at the surface of the steel plate. The concentration of longitudinal wave energy near the surface is shown by the principal lobe of the refracted signal. The maximum strength of the principle lobe is at an angle of refraction of 84°. There is a stronger lobe at 67°, but this is the first side lobe, which is not important in ultrasonic stress measurement. The lower relative amplitude of the principal lobe, as compared to the first side lobe, is mostly due to the incident energy that is lost by the reflection at the Plexiglas/steel interface. Also note that the longitudinal profile has multiple side lobes which trail off below 60°. The shear wave profile is much simpler. It consists of a single ultrasonic lobe at a 37° angle of refraction. This angle agrees closely with the Snell's Law calculation.

The longitudinal wave profile presented in this study is in excellent agreement with the theoretically predicted radiation patterns of Basatskaya *et al.*, as shown in Figure 12. Basatskaya[24] explains that when the incident longitudinal wave at the Plexiglas/steel interface equals 30°, "...the maximum displacement (i.e. amplitude) within the first principal lobe is even smaller than the corresponding maximum displacement within one side lobe." The L_{CR} wave transducer in this study is functioning slightly beyond the first critical angle; therefore, it is reasonable to assume that some of the energy that would generate the principal lobe is being reflected in the transducer at the interface. Basatskaya goes on to explain that as this incident angle is increased further so is the difference between the amplitudes of the principal and first side lobe. In this study, the refraction angle of both the principle and first side lobes is greater than those shown in Basatakaya's theoretical pattern; and, the difference in the amplitudes of these lobes is also correspondingly greater. Considering all of this, the distribution of refracted ultrasonic energy is remarkably similar.
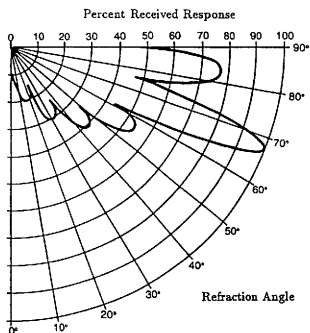
a) Longitudinal wave profile.
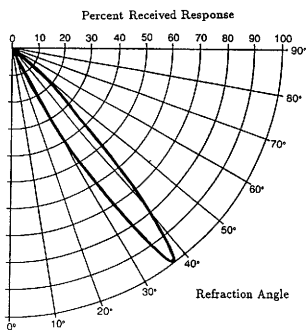
b) Shear wave profile.

Fig 11   The longitudinal and shear wave profiles of the L_{CR} wave transducer.
Frequency = 2.25 MHz and 25.4 mm (1.0 in) square.

Fig. 12 Theoretical longitudinal wave profile for a 30° incident longitudinal wave at a Plexiglas/steel interface. Frequency = 1 8 MHz and diameter = 18 mm (.71 in). Adapted from Basatskaya[24]

Beam Profiles of the Creeping Wave Transducer

The longitudinal and shear wave profiles of a commercial 2.25 MHz, dual-element focused creeping wave transducer were also measured with the beam profiling apparatus. The transducer is designed to generate high angle longitudinal waves for nondestructive inspection in steel specimens. This type of probe is extremely useful for near-surface testing[23]. It has separate transmitter and receiver crystals which are angled toward each other to provide a focusing effect. In the present research, only the transmitter of the creeping wave transducer was used. The beam profiles were measured by the profiling receivers coupled to the arc of the test plate.

The longitudinal and shear wave profiles of the creeping wave transducer are plotted in Figure 13 as a function of the refraction angle The longitudinal wave profile shows a strong lobe near the surface of the test specimen with the maximum strength

at 72° The location of this lobe indicates that it is the principal longitudinal lobe. The component of this lobe which is parallel to the surface, i.e. at 90° refraction angle, is identified as the creeping wave. In this study, the strength of the creeping wave was only 25% of the maximum received signal. Note that there also are some side lobes that trail off below 60°. These are similar to those seen in the L_{CR} wave transducer's profile but the relative amplitude is much lower. The relatively low strength of the side lobes is due to acoustic damping of the creeping wave transducer's crystal. The shear wave beam profile consists of a single lobe at an angle of refraction of 33°. This profile is also very similar to the L_{CR} wave transducer's shear profile with only a small change in the refraction angle The refraction angle of this shear wave corresponds to the Snell's Law prediction for a shear wave generated by mode conversion from a critical refracted longitudinal wave in steel

Röntgen Technische Dienst[29] has published in their commercial literature a schematic of the creeping wave transducer's radiation pattern in steel, as shown in Figure 14. The piezoelectric elements in the transducer are shown to be fixed at the first critical angle of refraction. The main compressional envelope, i.e. the principal lobe, is quoted in the literature to be at an angle of 74°, a slightly higher angle than measured here. The creeping wave is identified as the component of the principle lobe that is traveling along the surface. The schematic also shows that the creeping wave transducer excites a shear wave lobe at 33° as predicted by Snell's law. The experimental profiles presented in this research are in very close agreement with these published data.

Analysis of Results

The shear wave profiles of both the L_{CR} and creeping wave transducer are very similar, but not identical. The differences provide some useful information about the transducers. The angle of refraction at which the shear wave is excited by the L_{CR} wave probe is 4° greater than that of the creeping wave probe. This clearly
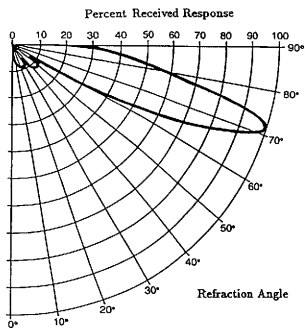
a) Longitudinal wave profile.
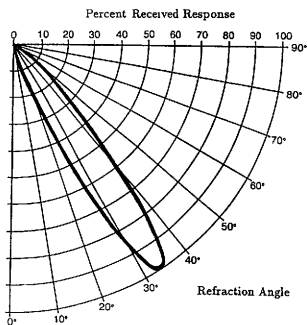
b) Shear wave profile.

Fig. 13. The longitudinal and shear wave profiles of the creeping wave transducer. Frequency = 2 25 MHz and 25.4 mm (1.0 in) square.
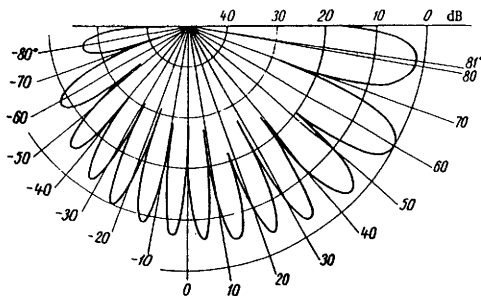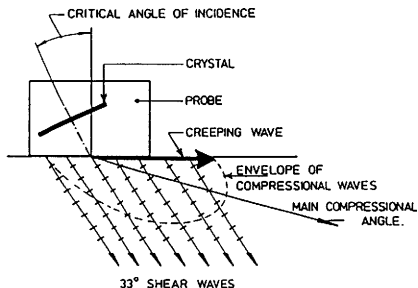
Fig. 14. Schematic of the creeping wave transducer's radiation pattern as published by Röntgen Technische Diest, BV. Frequency = 2.25 MHz. Reported by De Raad[29]

demonstrates that the incident angle of the L_{CR} wave transducer is greater than that of the creeping wave transducer, which is already at the first critical angle of refraction.

The creeping wave component identified in the longitudinal radiation pattern of the commercial creeping wave probe may also be identified in the longitudinal beam profile of the L_{CR} wave transducer. By definition, the creeping wave is the component of the principal lobe that is directed parallel to the surface of the test specimen, i.e. the angle of refraction equals 90°. The creeping wave generated by the L_{CR} wave probe has an amplitude equal to 50% of the maximum received signal. This is a greater percentage than that generated by the creeping wave probe. The higher amplitude of the critically refracted component of the L_{CR} wave transducer is directly related to the slightly increased incident angle. The L_{CR} wave probe is a stronger creeping wave transmitter because a larger portion of the principal lobe energy is actually being refracted along the surface of the specimen. This difference has been

observed. The creeping wave probe's signal decays rapidly making acoustoelastic stress measurements difficult; while, the L_{CR} wave probe's signal, as previously noted, has been used at distances of over 480 mm (19 in.).

The commercial creeping wave transducer is highly damped with backing material; whereas, the L_{CR} wave transducer is undamped by design. The effects of this damping are clearly evident in the longitudinal beam profiles. In comparison, the amplitudes of the multiple side lobes for the creeping wave probe trail off significantly below 60° while those for the L_{CR} wave probe remain strong. With the stronger undamped signal and the larger critically refracted component, the L_{CR} wave transducer is much better suited for acoustoelastic stress measurement. The creeping wave transducer generates a radiation pattern where the majority of the emitted ultrasonic energy is contained within a single compressional lobe oriented slightly into the material and a single trailing shear lobe. Thus, the creeping wave probe is much better suited for near-surface inspection where strong side lobes would confuse the interpertation.

The positions and relative amplitudes of the ultrasonic lobes presented in the beam profiles are well defined by the experimental data; whereas, the divisions between the lobes are not so well defined and required some extrapolation. The relatively large dimension of the profiling transducers, as compared to the width of these null depths produced some blurring of the received signal strengths. Smaller profiling transducers would have increased the resolution of these null depths. Nevertheless, the large amplitude changes observed in these experiments adequately document the beam characteristics of these two probes. The beam profiling technique presented in this chapter is a simple and accurate method for determining the beam profiles of ultrasonic transducers in a given test material.

RESIDUAL STRESSES IN THE PATCH WELDED PLATES

Two patch welded steel plates supplied by the DuPont Co. were used to evaluate the L_{CR} ultrasonic technique for residual stress measurement. The two large steel plates were patch welded in the center to create a residual stress field; and subsequently, one of the plates was stress relieved. Travel-time measurements of critically refracted longitudinal waves are used to determine the stress state of the plates and to estimate the stresses created by thermal contraction of the circular patch welds. The results indicate that the travel-times obtained with the L_{CR} ultrasonic technique can be used to distinguish between the stress relieved and non-stress relieved plates[30].

Consideration of the Weld Stress Measurement Parameters

The L_{CR} wave probe used in this study is a long device with three in-line L_{CR} wave transducers, as described previously, and a magnetic clamping system. The probe is configured with two receivers that are in-line with a single transmitter. Its overall length is about 635 mm (25 in.), as shown in Figure 15. The entire probe assembly was constructed at Texas A&M University and has a nominal operating frequency of 2.25 MHz.

When a L_{CR} wave pulse is excited in the steel plate by the transmitter, the velocity of this wave can be determined by the travel-time between the two receivers. Since the distance between the receivers is a constant, the acoustic velocity is inversely proportional to this travel-time. Consequently, the acoustoelastic relationship can be expressed in terms of travel-time. The tandem-catch arrangement minimizes the

Fig. 15. A photograph of the L_{CR} probe used in the patch weld residual stress research. Not shown to scale.

travel-time measurement errors that can be created by wave speed changes in the transducers or transmitter triggering uncertainty

To evaluate the stress state in steel plates, the effects on the wave speed of the residual stress, texture, and temperature in the plate must be established. Since the measured travel-time is proportional to the velocity, the acoustoelastic analysis may be performed on the differential travel-times. The model of the acoustoelastic parameters proposed by Bray et al[15] is expressed in terms of travel-time as

$$t = t^* + \Delta t_F + \Delta t_{RS} + \Delta t_{TX} + \Delta t_T \qquad (9)$$

where:

t – measured travel-time,

t^* – travel-time for a homogeneous, isotropic, stress free plate at a standard temperature,

Δt_F – travel-time effect of the applied force,

Δt_{RS} – travel-time effect of the residual stresses,

Δt_{TX} – travel-time effect of the material texture, and

Δt_T – travel-time effect of the temperature difference from the standard temperature

For stress measurement in welded plates, the change in travel-time due to applied force, Δt_F, may be redefined as Δt_{WS}, the change in travel-time due to the weld induced stress. The effect of the manufacturing induced residual stresses in the original plate remains Δt_{RS}. The travel-time in a typical as-manufactured steel plate without weld stresses and at a reference temperature may be expressed as:

$$t_o = t^* + \Delta t_{RS} + \Delta t_{TX} \tag{10}$$

This reference travel-time, t_o, represents the stress free travel-time of the material plus the changes required for manufacturing induced residual stress and material texture In this study, the reference travel-time is determined from measurements in a stress free portion of the patch welded plates. Combining Equations 9 & 10 yields an applicable equation for the change in travel-time due to the weld induced stress in the plate at any temperature:

$$\Delta t_{WS} = \Delta t_F = t - t_o - \Delta t_T \tag{11}$$

where t is the experimentally determined travel-time obtained from the welded plate that is being evaluated. With a knowledge of the weld induced change in travel-time and the appropriate acoustoelastic constant, the stress change created by the weld at any point in the plate may be calculated.

The relationship of measured L_{CR} wave change in travel-time to the corresponding change uniaxial stress is given by Egle and Bray[13] to be:

$$\Delta\sigma = \frac{E}{A_{11} * t_o}(t - t_o - \Delta t_T) \tag{12}$$

where $\Delta\sigma$ is the change in stress due to the weld While the assumption of an uniaxial stress field is not correct for the patch weld circumstance of the present study, the

stress field for many butt-weld arrangements may be approximated by an uniaxial field. As an estimation, the weld stresses in this study are calculated under the uniaxial assumption.

The Effects of Temperature and Texture

The effect of temperature on wave speed may be included, if the conditions require that this be done. For pearlitic steel, the linear effect of temperature on the velocity of longitudinal ultrasonic waves has been determined[16] to be $+0.55 \frac{m}{s \cdot {}^oC}$. For the probe used in this study, the temperature effect on the travel-time was calculated to be 0.0034 $\frac{\mu s}{{}^oC}$. With this value, Δt_T, is established for the conditions at the time the data were obtained. The range over which the temperature fluctuated during this experiment, 22.6^oC to 23.2^oC, produced no significant effect

One problem associated with using the acoustoelastic relationship for stress measurement is that nominally identical materials may exhibit slight differences in wave speeds and acoustoelastic constants. The wave speed variations may originate from texture as well as residual stresses. Differences in acoustoelastic constants most likely are caused by texture effects[10]. Where texture is relatively constant, however, the data indicate that stress differentials are measurable. Additionally, data collection and analysis schemes designed for specific applications may yield reasonable estimates of absolute stress levels.

Changes in the plates' material texture and the texture near to weld seams are thought to be a serious obstacle to using the acoustoelastic effect for stress measurement. This was not the case for two structural steel plates joined at the center by a longitudinal double vee groove weld, as reported by Leon-Salamanca et al[21,31] Data were obtained from the plates before and after heat treatment, using both the L_{CR} wave and neutron diffraction techniques. The effects of the stress relief were clearly shown by the L_{CR} wave data, but not by the neutron diffraction results which would have been affected by any change in texture. Since the heat treatment

did not affect the texture, the results indicate that the initial travel-time profiles were caused by the internal stress of the weld and not by the texture.

Experimental Design

The present study describes the evaluation of two patch welded steel plates which were supplied by the DuPont Co The test plates are made of 13 mm (0.5 in.) thick, ASTM A-516, Grade 60 Steel. Each plate is 120 cm (48 in) square and contains a circular patch weld at the center, as shown in Figure 16. The welded patch, R = 76 mm (3.0 in) creates a significant stress field in the plate One of the test plates was stress relieved after it was patch welded while the other was not. At the time of the testing, it was not known which plate had been stress relieved. The effects of the weld induced stress, localized residual stress and material texture on the travel-time of the L_{CR} waves were examined in this experiment.

The L_{CR} wave probe used in this study was configured in a pitch and tandem-catch arrangment. The initial pulse used to excite the transmitting transducer was generated by a Panametrics Ultrasonic Analyzer, Model 5052-UA. The received signals were digitized with a computer system called PCDAS, Personal Computer Data Acquisition System, which allowed 16 wave forms to be averaged for each travel-time measurement. This system uses an analog to digital converter capable of real-time sampling rates of 20 MHz. This is notable since the accuracy of the travel-time measurements is a direct function of the sampling rate of the data acquisition system. Overall accuracy in measuring the arrival times was felt to be at least 0.025 μs.

Theoretical analysis of patch welds predicts that the largest variation in the stress distribution will occur in the tangential component as a function of the radial distance[32]. Thus, the tangential travel-time measurements taken in this study along several radial directions were the ones most likely to detect the stress gradient created by the patch welds. The additional effect of texture induced anisotropy was also investigated by varying the direction of propagation of the L_{CR} waves.
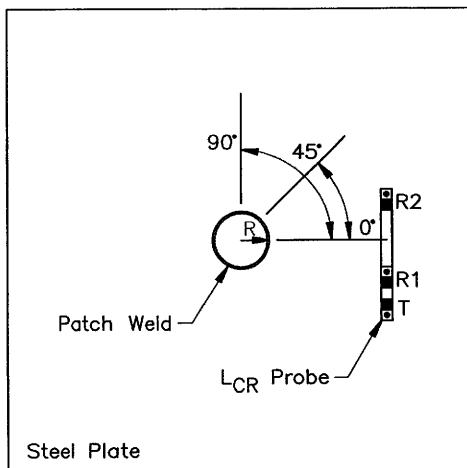
Fig. 16. Schematic of the L_{CR} probe and the patch welded plates showing the tangential orientation of the probe at $0°$ and the test plan geometry

A full factorial design is used in this experiment. A diagram of the test plan that was used for the travel-time measurements is shown in Figure 16. The L_{CR} wave probe was aligned tangential to the circular weld bead Travel-time measurements were taken along 3 radial directions ($0°$, $45°$, and $90°$) on each plate. Along each radial line, data were obtained at 19 distances. Near to the patch, where the stress effects would be greatest, data were obtained at 13 mm (0.5 in.) increments from the weld bead to a radial distance of 230 mm (9 in). From 230 to 380 mm (9 to 15 in.) data were taken at 25 mm (1.0 in.) intervals Temperature measurements were taken

at each location during the differential travel-time measurement procedure. This test plan produced 114 observations, 57 per plate A complete listing of the test data is presented in Appendix B. Randomization of the data acquisition process was used to eliminate bias and to insure random distribution of the experimental variance.

The ultrasonic travel-times obtained with the L_{CR} wave were used to distinguish between the stress relieved and non-stress relieved steel plates Figure 17 is a plot of the average differential travel-times for each plate as a function of the radial distance from the patch weld. Each data point is the mean travel-time of the three different angular samples at the same radial distance. A pattern in the data is apparent for plate 2. The data points farthest from the weld are relatively flat. Approaching the weld, there is a minimum travel-time at 152 mm (6.0 in) which steeply rises to a peek at the weld radius, 76 mm (3 in.). While there is scatter in the data for both plates, no distinctive minimum or maximum can be found for the plate 1.

The data pattern presented for plate 2 corresponds well to the theoretical predictions for the tangential weld stress distribution that would be created by a circular patch weld in a larger plate[32]. A region of high tangential, tensile stresses exist at the weld due to circumferential shrinkage of the weld metal These stresses may be as high as the yield strength of the material. Farther out from the patch weld, a region of lower tangential, compressive stresses exist due to radial shrinkage of the patch weld. Beyond this compressive region, a stress free area exists where the material is not affected by the patch weld. This region may be used to determine the stress free ultrasonic reference velocity for the material. All of these regions may be distinguished in the experimentally determined tangential travel-time distribution of the non-stress relieved plate 2. The results indicate that plate 1 was stress relieved while plate 2 was profiled in the as welded condition.
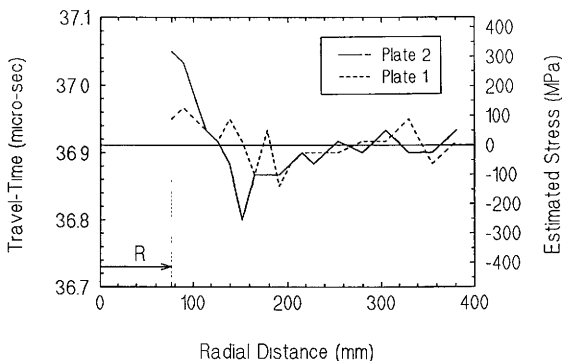
Fig. 17. Average differential travel-times for the L_{CR} waves traveling tangentially to a circular patch weld, R, as a function of radial distance for a stress relieved plate (1) and non-stress relieved plate (2). Estimated stress based on uniaxial stress field assumption.

Estimation of the Weld Induced Stresses

By assuming that the mean travel-time data in the region from 230 mm to 380 mm (9 to 15 in) represent a stress free reference travel-time, the relative change in stress at any point on the plate may be estimated from travel-time measurements at that point with Equation 12. The mean stress free travel-times for plates 1 and 2 were 36.9119 μs and 36.9095 μs respectfully; thus, yielding an average stress free travel-time, t_o, of 36.911 μs with a standard deviation of 0.056 μs. The greatest difference between this stress free reference travel-time and a experimentally measured travel-time was at the weld in plate 2. Applying Equation 11 at this point yields:

$$\Delta t_{WS} = t - t_o - \Delta t_T = 0.139 \ \mu s$$

which is the largest change in travel-time due to the weld induced stress   The temperature range during this experiment produced no significant change in L_{CR} wave speed, therefore, effect of temperature, Δt_T, was assumed to be zero.

From Egle and Bray[13], the L_{CR} wave acoustoelastic constant, A_{11}, for pearlitic steel is 2.45. Young's modulus for the plate steel is 207 GPa (30 X 10^6 psi) For approximation purposes, it will be assumed that the present data from the patch welded plates is representative of data from a uniaxial stress field. Thus, maximum change in stress due to the weld may be calculated using Equation 12

$$\Delta\sigma = \frac{207 \ X \ 10^9}{(2.45)(36.911)}(0.139) = 318 \ MPa \ (46 \ ksi)$$

This value exceeds the minimum yield stress of 262 MPa (38 ksi) for the structural steel used for the patch welded plates. The calculation, however, is based on the assumption of a uniaxial stress state. In reality, a biaxial stress state actually exists in the patch welded plates Therefore, the stress scale shown in Figure 17 is only an estimation of the tangential stresses that the patch welds create.

The stress distribution presented in Figure 17 agrees well with theoretical predictions for tangential, residual stresses created by circular patch weld   Figure 18 shows a typical patch welded plate and the theoretical residual stress distribution associated with it. Note that a biaxial stress distribution is actually created in the weld effected region by the circumferential and radial shrinkage of the patch weld[32]. The tangential stress distribution, which displays a larger range of stress levels, was investigated in this research because it was more likely to be detected.

Statistical Analysis of Data

Data were analyzed using an analysis of variance (ANOVA) and a least sig-nificant difference T test, procedures widely used for identifying the significant independent variables within data sets and comparing pairs of means with equal variances[33,34]. The analysis of variance procedure partitions the total variation in a
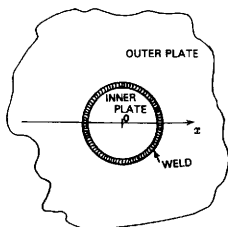
a)Circular patch-weld
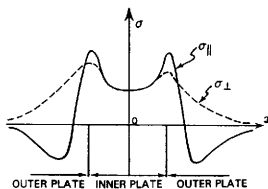
b)Distribution of residual stresses
in a patch-welded plate.

Fig. 18. Theoretical distribution of residual stresses in a circular patch welded
plate where $\sigma_{\parallel}$ and $\sigma_{\perp}$ are the tangential and radial stresses, respectively.
Adapted from Masubuchi[32].

measured response, such as travel-time, into components which can be attributed to
recognizable sources of variation[35]. Significant factors within data sets are indicated
by a F value statistic, which is the ratio of the variation attributed by the given
treatment (factor) to the variation attributed by random experimental error.

A significance level of one percent ($\alpha = 01$) is selected for this analysis. The
significance level, α, indicates the probability that a variable will be identified as

significant when, in truth, it is not. For a given significance level, the number of treatments (k) and the total number of data points (N) establishes a minimum critical F value, which may be obtain from statistical tables. The statistical computer program used for this analysis, SAS, went one step further. It calculated the actual significance probability, Pr, corresponding to each F value If this calculated significance probability is less than or equal to the selected level, α, the null hypothesis, that all of the samples are the same, may be rejected When null hypothesis is rejected ($Pr > F$), the conclusion is that the treatment had a significant effect on the measured response. Otherwise, the treatments are assumed to be the same.

The data for the present investigation are first analyzed to detect any variation with radial angle in the stress free region. Tables 1 and 2 show the ANOVA results for data obtained in the unstressed region at the three angles in plates 1 and 2, respectively In both cases the significance probability, Pr, is greater than the selected significance level, $\alpha = 0.01$. Thus, there is a 99% confidence that there are no significant differences by angle in the unstressed regions of the plates Further, Table 3 shows the ANOVA results comparing the stress free regions of the two plates. Again, the statistics indicates that the travel-times in the unstressed regions of the two plates are not significantly different. Thus by angle and plate, there is no detectable difference in the mean stress free reference travel-time for the two plates.

To determine if significant differences exist in any region of plates 1 and 2, an analysis of variance by radial distance is run in both plates. The ANOVA results are shown in Tables 4 and 5. For plate 1 (Table 4), the significance probability is greater than the selected level, indicating that there is no significant differences in travel-time by radius. For plate 2 (Table 5), however, the results indicate that significant

Table 1. Analysis of variance (ANOVA) of travel-times by angle in the stress free region of plate 1, $\alpha = 0.01$

Source	DF	SS	MS	F value	Pr>F
Angle	2	0.0267	0.0133	3.54	0.0506
Error	18	0.0678	0.0038		
N	20	0.0945			

Table 2. Analysis of variance (ANOVA) of travel-times by angle in the stress free region of plate 2, $\alpha = 0.01$

Source	DF	SS	MS	F value	Pr>F
Angle	2	0.0074	0.0037	2.58	0.1032
Error	18	0.0257	0.0014		
N	20	0.0331			

differences in the travel-time do occur with radius, since the probability is less than selected significance level, $\alpha = 0.01$.

Unfortunately, the ANOVA procedure does not tell us at which of the radial distances in plate 2 may the travel-times be regarded as significantly different from the others. Therefore, a least significant difference T test is used to identifying the differences in data set. A significance level of one percent, $\alpha = 0.01$, is again selected. The results of the T test are reported in groupings of means signified by different letters, starting with "A". Where significantly different data groupings are found, these are identified with different letters. Means within a group may also be different, but, we cannot claim this with a 99% confidence.

Table 3.   Analysis of variance (ANOVA) of travel-times by plate in the stress free region of the plates, $\alpha = 0.01$

Source	DF	SS	MS	F value	Pr>F
Plate	1	0.00006	0.00006	0.02	0.8920
Error	40	0.1276	0.0032		
N	41	0.1277			

Table 4.   Analysis of variance (ANOVA) of travel-times by radial distance for plate 1, $\alpha = 0.01$

Source	DF	SS	MS	F value	Pr>F
Radius	18	0.0524	0.0029	0.60	0.8739
Error	38	0.1833	0.0048		
N	56	0.2358			

Table 5.   Analysis of variance (ANOVA) of travel-times by radial distance for plate 2, $\alpha = 0.01$

Source	DF	SS	MS	F value	Pr>F
Radius	18	0.1860	0.0103	3.10	0.0016
Error	38	0.1267	0.0033		
N	56	0.3126			

Table 6 shows the T test groupings of the means for all of the data collected from plate 2. A graphical representation of these groupings are shown in Figure 19. The smallest group, A, contains the four points nearest to the weld having the longest travel-times, as well as two in the outer regions Group C contains all of the points in the assumed stress free region of the plate. Group D includes points with the shortest travel-times and particularly the minimum at 152 mm. These groups corresponds well to the theoretical predictions for the tangential stress distribution in a patch-welded plate.

Table 6.   Groupings by radius from the least significant difference T test for the mean travel-times in plate 2, $\alpha =0.01$

Grouping			Mean (µs)	N	Radius (mm (in))
	A		37.050	3	76.2 (3.0)
B	A		37.033	3	88.9 (3.5)
B	A	C	36.983	3	101.6 (4.0)
B D	A	C	36.933	3	114.3 (4.5)
B D	A	C	36.933	3	381.0 (15.0)
B D	A	C	36.933	3	304.8 (12.0)
B D	A	C	36.917	3	127.0 (5.0)
B D	A	C	36.917	3	254.0 (10.0)
B D		C	36.900	3	279.4 (11.0)
B D		C	36.900	3	355.6 (14.0)
B D		C	36.900	3	330.2 (13.0)
B D		C	36.900	3	215.9 (8.5)
B D		C	36.883	3	139.7 (5.5)
B D		C	36.883	3	203.2 (8.0)
B D		C	36.883	3	228.6 (9.0)
D		C	36.867	3	177.8 (7.0)
D		C	36.867	3	165.1 (6.5)
D		C	36.867	3	190.5 (7.5)
D			36.800	3	152.4 (6.0)

Several important observations may be made from the data analysis First, in the stress free region from 230 mm to 380 mm, the manufacturing induced residual stresses and texture in the plate should dominate over weld induced stresses. The
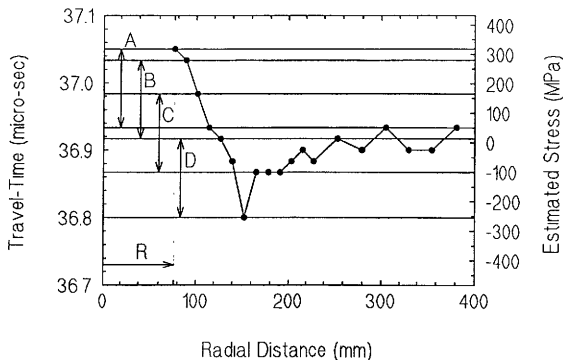
Fig. 19. T test grouping by radius of the mean differential travel-times for the L_{CR} waves propagating in the non-stress relieved plate 2.

analysis of data in this region show no significant differences in travel-times by angle or plate. These two findings indicate that the L_{CR} wave data are not significantly affected by texture nor localized residual stress in these plates.

The significantly different travel-time data that is found for the non-stress relieved plate in the region near the weld (region A) indicates that the L_{CR} ultrasonic technique is capable of distinguishing stress relieved welded steel plates from those that have not been stress relieved. While the increase is much larger for plate 2, both plates show some increase in the travel-time at the weld and in the small area near to it. These results clearly show that plate 1 was stress relieved but may also indicate that this stress relief may not have been complete.

The scatter which appears in the data could be derived from several sources, including local residual stresses and texture as previously discussed Most likely, much of this scatter is a result of random experimental error in the travel-time picks

and variations in the acoustic coupling of the L_{CR} probe. The length of the probe used in this study caused some difficulty in coupling it to the plates. A shorter probe configuration would, most likely, reduce these coupling induced variations.

Applications of the L_{CR} Ultrasonic Technique

The previously cited results on the welded plates suggest an immediately available procedure that can determine the presence or absence of high stresses in a weld and in the surrounding area[21]. The procedure is to obtain a travel-time profile across the region being investigated, starting at an assumed stress free reference point that is away from the weld affected zone Probe orientation is held constant with respect to the plate's rolling direction to control the effect of the texture on the ultrasonic velocity. A characteristic pattern in the travel-time profile would indicate that the part has not been stress relieved. The absence of a significant travel-time pattern would indicate a stress relieved condition. Without question, further research is needed to establish full confidence in the ability of the technique to measure weld stresses. Nonetheless, the results obtained thus far show that the L_{CR} method can be used to detect weld induced stresses.

In 1978, Fukuoka *et al*[36] used a "sing-around" acoustic birefringence technique and dissectioning to evaluate the residual stress distribution in patch welded circular plates made of mild steel. Those findings are in excellent agreement with the results obtained in this research. Fukuoka *et al* concluded from his research that "... acoustoelastic stress analysis seems to be one of the most promising techniques for nondestructive stress analysis, although there are still many difficult problems to overcome, notably those of transducer-coupling materials and separation of preferred orientation effects." The shear wave acoustic birefringence technique, as in the previously mentioned study, uses the travel-time change of the multiple echoes propagating across the thickness of the sample. Clearly, this technique is limited to

fully isotropic material having highly parallel sides. Moreover, the stresses measured will be the average through the thickness, and not indicative of any gradient

Since the L_{CR} ultrasonic technique is less sensitive to material texture and more sensitive to stress, the variations due to the preferred orientation effect are much less pronounced. Additionally, the possibility of measuring stress gradients through the choice of different excitation frequencies is intriguing[37]. Furthermore, the L_{CR} technique does not impose any strict geometric limitations on the test specimens. The results of this research seem to indicate that the L_{CR} ultrasonic technique is the most promising acoustoelastic method for nondestructive stress analysis since it has overcome many of the problems associated with the birefringence technique.

CONCLUSIONS

Residual stresses always have been a nemesis of sound engineering design. Uncertainty about the residual stress state has led to significant over design in many engineering structures[38]. Wylde[39] specifically describes the influence of residual stresses on designing welded structures. The general conclusion is that in the absence of information about the residual stress, the safe assumption is that residual stresses may be as high as the yield strength of the material. Clearly, a knowledge of the residual stresses would be beneficial to engineering design. More specifically, knowledge if a weld has been properly stress relieved would remove a large portion of the design uncertainty that now exists

The acoustic techniques are based on the acoustoelastic effect which correlates the stress field in a material to changes in the ultrasonic wave speed. This linear relationship of stress to ultrasonic velocities is relatively small, on the order of a few hundreds of a percent[9]; and yet, it has been used successfully for many years to measure bulk and near-surface stresses. As research on the nondestructive measurement of stress has evolved over the years, it has become clear that the critically refracted longitudinal wave technique offers some distinct advantages over other methods. Since the L_{CR} wave is a bulk wave which travels just below the surface of the material, it is sensitive to a stress field in a finite thickness and not just at the surface. Also important is that in comparison to the shear wave, the L_{CR} wave is the more sensitive to stress and, yet, it is less sensitive to material texture[13,19,25].

The results show that the L_{CR} ultrasonic, stress measurement technique can quantitatively distinguish between stress relieved and non-stress relieved plates. Furthermore, it appears that the degree to which a plate or weld is stress relieved may also be indicated. Once a reference travel-time is determined from a stress free region of a plate, the relative stress level at any other point on the plate may be estimated from travel-time measurements at that point and the appropriate acoustoelastic constant. The patch welded plate's stress distribution that is approximated from the

experimentally measured travel-times in this study corresponds well with other experimental and theoretical predictions.

The L_{CR} ultrasonic technique used in this study has shown an ability to indicate stress conditions in a variety of materials. The earlier studies applying the technique to stress measurement in railroad rail[13,15,16,20] were continued by Polish investigators[40,41]. They report success in monitoring manufacturing induced stresses as well as thermal induced stress changes in rail installed in the track. Also, the technique has demonstrated an ability to measure stress in castings made from ductile cast iron[42,43]. In another application, the L_{CR} technique was used to determine the stress distribution in a shrunk fit retaining ring installed in a turbine rotor at an electric generating station[44]. As interest in the L_{CR} ultrasonic technique expands, further applications will surely develop.

The overall precision of stress measurement with the L_{CR} ultrasonic technique is dependent on the accuracy of the system used to obtain travel-time data. Where the system used for the present study had an accuracy of 0.025 μs, systems presently available are capable of measurements within 0.001 μs. Further, a new smaller probe design as used in the ductile cast iron studies[42,43] should improve the overall precision of the system by reducing the random scatter caused by variations in the acoustic coupling.

Uncertainty which exists in using the L_{CR} ultrasonic technique generally rests in unanticipated variations in the parameters affecting the acoustic travel-times, namely the acoustoelastic constant, the presence of any external forces, and material texture. Field experience in using this technique has shown that variations are to be expected. Laboratory experimentation will continue to quantify the acoustoelastic constants for other materials, to develop more robust data acquisition methodologies, as well as to improve accuracy and precision of the travel-time measurement systems.

REFERENCES

1 **Nelson, D.** 'Finding the Stress Hidden in Parts' *J Machine Design* **58** (1986) p 125

2 **Mordfin, L.** 'Measurement of Residual Stresses: Problems and Opportunities' in *Residual Stress for Designers and Metalurgists* ed L.J. Vande Wall, American Society for Metals, Metals Park, Ohio (1980) p 189

3 **Treuting, R.G., Lynch, J.J., Wishart, H.B. and Richards D.G.** *Residual Stress Measurements* American Society for Metals, Metals Park, Ohio (1952)

4 **Musubuchi, K.** 'Residual Stresses and Distortion' in *Welding, Brazing, and Soldering, Metals Handbook* vol VI, Ninth Edition, American Society for Metals, Metals Park, Ohio (1983) p 856

5 **Wohlfahrt, H.** 'Residual Stresses Due to Welding: Their Origin, Calculation and Evaluation' in *Residual Stresses* Proceedings of the 1983 European Conference on Residual Stresses, ed E. Macherauch and V. Hauk, Informationsgesellschaft, Verlag, Germany (1986) p 81

6 **Leon-Salamanca, T.** 'Ultrasonic Measurement of Residual Stress in Steels Using Critically Refracted Longitudinal Waves (L_{CR})' *Ph.D. Dissertation* Dept. of Mechanical Engineering, Texas A&M University (1988)

7 **Wulpi, D.J.** *Understanding How Components Fail* American Society for Metals, Metals Park, Ohio (1985) p 63

8 **Proctor, T.M., Jr.** 'Introduction to Papers Presented at the Symposium of Ultrasonic Measurement of Stress' *J Test & Eval* **10** (1982) p 199

9 **Schnieder, E. and Gobbels, K.** 'Nondestructive Evaluation of Residual Stress States Using Ultrasonic Techniques' in *Residual Stresses* Proceedings of the 1983 European Conference on Residual Stresses, ed E. Macherauch and V. Hauk, Informationsgesellschaft, Verlag, Germany (1986) p 247

10 **Thompson, R.B., Smith, J.F. and Lee S.S.** 'Effects of Microstructure on Acoustoelastic Measurements of Stress' in *Nondestructive Evaluation, Application to Material Processing* ed O. Buck and S Wolf, American Society of Metals, Metals Park, Ohio (1894) p 137

11 **Allen, D.R., Cooper, W.H.B., Sayers, C.M. and Silk, M.G.** 'The Use of Ultrasonics to Measure Residual Stress' in *Research Techniques in NDT* vol VI, ed R.S. Sharpe, Academic Press, London (1982) p 151

12 **Pao, Y.H., Sachse, W. and Fukuoka, H.** 'Acoustoelasticity and Ultrasonic Measurements of Residual Stresses' in *Physical Acoustics* vol XVII, ed W.P. Mason and R.N. Thurston, Academic Press, New York (1984) p 61

13 **Egle, D.M. and Bray, D.E.** 'Measurement of Acoustoelastic and Third–Order Elastic Constants in Rail Steel' *J Acoust Soc Am* **60** (1976) p 741

14 **Hughes, D.S. and Kelly, J.L.** 'Second–Order Elastic Deformation of Solids' *Physical Review* **92** (1953) p 1145

15 **Bray, D.E. and Leon-Salamanca, T.** 'Zero-Force Travel-Time Parameters for Ultrasonic Head-Waves in Railroad Rail' *Mater Eval* **43** (1985) p 854

16 **Egle, D.M. and Bray, D.E.** 'Nondestructive Measurement of Longitudinal Rail Stresses: Application of the Acoustoelastic Effect to Rail Stress Measurement' *Federal Railroad Administration Report No FRA/ORD–77/341* Pb–281164, NTIS, Springfield, Virginia (1978)

17 **Musgrave, M.J.P.** *Crystal Acoustics: Introduction to the Study of Elastic Waves and Vibrations in Crystals* Holden-Day, San Francisco, California (1970)

18 **Arora, A.and James, M.R.** 'Ultrasonic Measurement of Residual Stress in Textured Materials' *J Test & Eval* **10** (1982) p 212

19 **Bray, D.E. and Egle, D.M.** 'Ultrasonic Studies of Anisotropy in Cold-Worked Layer of Used Railroad Rail' *Metal Science* **15** (1981) p 574

20 **Egle, D.M. and Bray, D.E.** 'Application of the Acousto-elastic Effect to Rail Stress Measurement' *Materials Evaluation* **37** (1979) p 41

21 **Bray, D.E., Leon-Salamanca, T. and Junghans, P.G.** 'Application of the L_{CR} Ultrasonic Technique for Evaluation of Post-Weld Heat Treatment in Steel

Plates' in *Nondestructive Evaluation: Planning and Application* Proceedings of the 1989 ASME Pressure Vessels and Piping Conference, ed. R D. Streit, Honolulu, Hawaii (1989) p 191

22 **Ermolov, I.N., Razygraev, N.P. and Shcherbinskii V.G.** 'The Use of Head-Type Acoustic Waves for Ultrasonic Monitoring' *Sov J NDT* **14** (1978) p 27

23 **Smith, P.H.** 'Practical Application of Creeping Waves' *Br J NDT* **29** (1987) p 318

24 **Basatskaya, L.V. and Ermolov, I.N.** 'Theoretical Study of Ultrasonic Subsurface Waves in Solid Media' *Sov J NDT* **16** (1980) p 524

25 **Bray, D.E. and Stanley, R.K.** *Nondestructive Evaluation: A Tool for Design, Manufacturing, and Service* McGraw-Hill, New York (1989)

26 **Razygraev, N.P. and Ermolov, I.N.** 'Probes for Surface-Layer Inspection by Means of Head Waves' *Sov J NDT* **17** (1981) p 40

27 **Langenberg, K.J., Fellinger, P. and Makklein, R.** 'On the Nature of the So-called Subsurface Longitudinal Wave and/or the Surface Longitudinal "Creeping" Wave' *Res NDE* **2** (1990) p 59

28 **Junghans, P.G. and Bray, D.E.** 'Beam Characteristics of High Angle Longitudinal Wave Probes' in *NDE: Applications, Advanced Methods, and Codes and Standards* Proceedings of the 1991 Pressure Vessels and Piping Conference, ed R.N. Pangborn *et al*, Am Soc Mech Engr, New York **219** (1991) p 39

29 **De Raad, J.A.** 'Ultrasonic Probes and Accessories for Pipescanning Systems' contributed to 1986 EPRI NDE Center Workshop/Technology Fair, Röntgen Technische Dienst, BV., Rotterdam, Netherlands (1986)

30 **Bray, D.E. and Junghans P.G.** 'Application of the L_{CR} Ultrasonic Technique for Evaluation of Post-weld Heat Treatment in Steel Plates' *NDT International* (In Review)

31 Leon-Salamanca, T. and Bray, D.E. 'Ultrasonic Mesurement of Residual Stress in Steels using Critically Refracted Longitudinal Waves (L_{CR})' Proceeding of 1990 SEM Spring Conference on Experimental Mechanics, Albuquerque, New Mexico, Soc Experimental Mechanics (1990) p 271

32 Masubuchi, K. *Analysis of Welded Structures* First Edition, Pergamon Press, New York (1980) p 203

33 Montgomery, D.C. *Design and Analysis of Experiments* Third Edition, John Wiley & Sons, New York (1991)

34 Hough, C.L. 'The Effect of Back Rake Angle on the Performance of Small-Diameter Polycrystalline Diamond Rock Bits: Anova Tests' *J Energy Resources Tech* 108 (1986) p 305

35 Milton, J.S. and Arnold, J.C. *Probability and Statistics in Engineering and Computing Sciences* First Edition, McGraw-Hill, New York (1986)

36 Fukuoka, H., Toda, H. and Yamane, T. 'Acoustoelastic Stress Analysis of Residual Stress in a Patch-welded Disk' *Experimental Mechanics* 18 (1978) p 277

37 Leon-Salamanca, T. and Reinhart, E. 'Surface Residual Stress Analysis of Metals and Alloys' Final Report for Dept. of the Navy, Naval Air Systems Command, Reinhart & Associates Inc., Austin, Texas (1992)

38 Shigley, J.E. and Mischke, C.R. *Mechanical Engineering Design* Fifth Edition, McGraw-Hill, New York (1989)

39 Wylde, J.E. 'The Influence of Residual Stresses on the Fatigue Design of Welded Steel Structures," in *Residual Stress in Design, Process and Materials Selection* ed W.B. Young, American Society of Metals, Metals Park, Ohio (1987) p 85

40 Brokowski, A. and Deputat, J. 'Ultrasonic Measurements of Residual Stresses in Rails' vol I, Proceeding of the 11th World Conference on Nondestructive Testing, American Society for Nondestructive Testing, Columbus, Ohio (1985) p 592

41 **Szelazek, J.** 'Ultrasonic Measurement of Thermal Stresses in Continuously Welded Rail' *NDT & E International* **25** (1992) p 77

42 **Srinivasan, M.N., Bray, D.E., Junghans, P.G. and Alagarsamy, A.** 'Critically Refracted Longitudinal (L_{CR}) Wave Technigue: A New Tool for Measurement of Residual Stresses in Castings' *AFS (American Foundrymens Society) Transactions* **99** (1991) p 265

43 **Srinivasan, M.N., Chundu, S.N., Bray, D.E. and Alagarsamy, A.** 'Utrasonic Technique for Residual Stress Measurement in Ductile Iron Continuous Cast Round Bars' *J Test & Eval* **20** (1992) p 331

44 **Leon Salamanca, T.** 'An Utrasonic Method for Stress Measurement in Structures' contributed to 1988 EEI Metallurgy and Piping Task Force, Reinhart & Associates Inc., Austin, Texas (1988)

APPENDIX A

BEAM PROFILING DATA

L_{CR} WAVE TRANSDUCER DATA

ANGLE	LONGITUDINAL[1] AMPLITUDE			SHEAR[2] AMPLITUDE		
90.0	50	47	45	0	0	0
87.5	57	57	60	0	0	0
85.0	57	72	75	0	0	0
82.5	75	77	77	0	0	0
80.0	72	72	72	0	0	0
77.5	65	60	62	0	0	0
75.0	62	57	62	0	0	0
72.5	67	57	67	0	0	0
70.0	80	85	80	0	0	0
67.5	100	97	97	0	0	0
65.0	90	87	90	0	0	0
62.5	67	65	70	0	0	0
60.0	57	57	60	0	0	0
57.5	55	57	55	0	0	0
55.0	50	52	52	2	2	0
52.5	50	50	47	7	7	2
50.0	47	47	47	10	7	7
47.5	42	42	42	17	12	12
45.0	40	40	40	37	37	20
42.5	37	37	37	57	52	40
40.0	37	37	32	70	72	62
37.5	32	30	35	92	102	85
35.0	32	30	30	92	87	80
32.5	30	27	30	55	57	55
30.0	30	27	27	30	20	20
27.5	27	22	22	10	10	5
25.0	25	20	20	5	5	0
22.5	22	20	20	0	2	0
20.0	22	20	17	0	0	0
17.5	20	17	17	0	0	0
15.0	20	17	17	0	0	0
12.5	20	15	12	0	0	0
10.0	15	12	12	0	0	0
7.5	15	12	12	0	0	0
5.0	12	12	12	0	0	0
2.5	12	12	12	0	0	0
0.0	10	10	10	0	0	0

1 - PERCENT FULL SCREEN LONGITUDINAL RESPONSE
2 - PERCENT FULL SCREEN SHEAR RESPONSE

CREEPING WAVE TRANSDUCER DATA

ANGLE	LONGITUDINAL AMPLITUDE				
90.0	15	10	15	15	15
85.0	30	25	25	35	35
80.0	35	50	40	55	60
75.0	55	70	55	65	75
70.0	65	75	55	75	80
65.0	50	60	40	55	60
60.0	30	25	20	25	30
55.0	15	15	10	10	10
50.0	10	10	10	10	10
45.0	5	5	8	8	10
40.0	5	5	8	5	7
35.0	5	5	5	5	7
30.0	5	5	5	5	5
25.0	5	5	5	5	5
20.0	5	2	3	3	5
15.0	5	2	2	2	3
10.0	0	0	0	2	0
5.0	0	0	0	0	0
0.0	0	0	0	0	0

ANGLE	SHEAR AMPLITUDE				
90.0	0	0	0	0	0
85.0	0	0	0	0	0
80.0	0	0	0	0	0
75.0	0	0	0	0	0
70.0	0	0	0	0	0
65.0	0	0	0	0	0
60.0	0	0	0	0	0
55.0	0	5	5	5	5
50.0	5	10	15	10	18
45.0	22	20	25	25	40
40.0	55	55	65	90	90
35.0	90	90	85	105	105
30.0	85	90	95	100	100
25.0	35	40	35	40	50
20.0	20	20	22	20	18
15.0	5	5	5	5	10
10.0	0	0	0	0	0
5.0	0	0	0	0	0
0.0	0	0	0	0	0

APPENDIX B

PATCH WELDED PLATES DATA

OBS[1]	RADIUS[2]	ANGLE[3]	TEMP[4]	TT1[5]	TT2[6]	PLATE[7]
60	3.0	90	73.2	48.79	85.64	1
43	3.5	90	73.4	48.64	85.59	1
53	4.0	90	73.5	48.69	85.54	1
11	4.5	90	73.6	48.69	85.54	1
70	5.0	90	73.2	48.64	85.49	1
17	5.5	90	73.5	48.59	85.49	1
81	6.0	90	73.6	48.59	85.49	1
42	6.5	90	73.3	48.64	85.49	1
71	7.0	90	73.3	48.59	85.54	1
6	7.5	90	73.0	48.69	85.54	1
10	8.0	90	73.2	48.64	85.49	1
59	8.5	90	73.2	48.79	85.59	1
8	9.0	90	73.1	48.74	85.49	1
69	10.0	90	73.2	48.74	85.54	1
52	11.0	90	73.5	48.59	85.49	1
24	12.0	90	73.4	48.59	85.49	1
18	13.0	90	73.5	48.54	85.49	1
82	14.0	90	73.5	48.64	85.44	1
23	15.0	90	73.5	48.54	85.49	1
108	3.0	45	73.2	48.64	85.69	1
109	3.5	45	73.2	48.89	85.89	1
105	4.0	45	73.0	48.84	85.84	1
113	4.5	45	73.5	48.89	85.89	1
110	5.0	45	73.4	48.69	85.64	1
112	5.5	45	73.5	48.69	85.64	1
107	6.0	45	73.2	48.84	85.79	1
104	6.5	45	72.8	48.69	85.54	1
115	7.0	45	73.6	48.79	85.64	1
111	7.5	45	73.4	48.69	85.59	1
106	8.0	45	73.1	48.89	85.79	1
114	8.5	45	73.5	48.89	85.84	1
51	9.0	45	73.6	48.69	85.64	1
13	10.0	45	73.7	48.64	85.54	1
31	11.0	45	73.2	48.64	85.59	1
38	12.0	45	73.2	48.64	85.54	1
61	13.0	45	73.2	48.79	85.79	1
32	14.0	45	73.2	48.69	85.54	1
2	15.0	45	72.7	48.64	85.54	1
29	3.0	0	73.1	48.69	85.64	1
83	3.5	0	73.5	48.69	85.64	1
49	4.0	0	73.4	48.64	85.64	1
4	4.5	0	72.6	48.64	85.59	1
40	5.0	0	73.3	48.69	85.64	1
62	5.5	0	73.2	48.64	85.64	1

1 - RANDOM OBSERVATION ORDER OF THE TRAVEL-TIME MEASUREMENTS
2 - RADIAL DISTANCE FROM THE CENTER OF THE PATCH WELD IN INCHES
3 - ANGULAR DIRECTION IN DEGREES
4 - TEMPERATURE AT TIME OF MEASUREMENT IN DEGREES FAHRENHEIT
5 - TRAVEL-TIME TO THE FIRST RECEIVER IN MICROSECONDS
6 - TRAVEL-TIME TO THE SECOND RECEIVER IN MICROSECONDS
7 - AS WELDED AND STRESS RELIEVED PLATE DESIGNATION

OBS	RADIUS	ANGLE	TEMP	TT1	TT2	PLATE
12	6.0	0	73.6	48.69	85.59	1
84	6.5	0	73.5	48.64	85.54	1
7	7.0	0	73.1	48.64	85.64	1
72	7.5	0	73.3	48.74	85.54	1
3	8.0	0	72.6	48.64	85.54	1
103	8.5	0	72.9	48.59	85.54	1
41	9.0	0	73.3	48.59	85.59	1
39	10.0	0	73.3	48.59	85.59	1
74	11.0	0	73.3	48.69	85.59	1
30	12.0	0	73.2	48.59	85.54	1
85	13.0	0	73.5	48.59	85.49	1
50	14.0	0	73.5	48.59	85.59	1
73	15.0	0	73.3	48.64	85.54	1
86	3.0	90	73.1	48.64	85.69	2
37	3.5	90	72.9	48.59	85.64	2
16	4.0	90	73.4	48.59	85.59	2
26	4.5	90	73.0	48.59	85.54	2
67	5.0	90	73.0	48.59	85.54	2
78	5.5	90	73.1	48.59	85.49	2
54	6.0	90	72.7	48.59	85.49	2
45	6.5	90	73.2	48.59	85.49	2
87	7.0	90	73.1	48.59	85.49	2
36	7.5	90	72.9	48.59	85.44	2
68	8.0	90	72.9	48.59	85.49	2
5	8.5	90	72.7	48.59	85.49	2
79	9.0	90	73.1	48.59	85.49	2
25	10.0	90	73.1	48.59	85.49	2
22	11.0	90	73.1	48.59	85.49	2
44	12.0	90	73.2	48.59	85.49	2
55	13.0	90	72.8	48.54	85.44	2
35	14.0	90	72.9	48.59	85.44	2
80	15.0	90	73.1	48.54	85.49	2
95	3.0	45	72.8	48.74	85.84	2
98	3.5	45	72.9	48.64	85.69	2
101	4.0	45	73.0	48.64	85.64	2
99	4.5	45	72.9	48.64	85.59	2
97	5.0	45	72.9	48.64	85.59	2
92	5.5	45	72.7	48.64	85.54	2
84	6.0	45	72.8	48.64	85.54	2
102	6.5	45	73.0	48.64	85.54	2
91	7.0	45	72.7	48.64	85.54	2
93	7.5	45	72.7	48.64	85.54	2
96	8.0	45	72.8	48.69	85.59	2
100	8.5	45	72.9	48.59	85.54	2
56	9.0	45	72.8	48.79	85.64	2
66	10.0	45	72.9	48.64	85.59	2
21	11.0	45	73.0	48.64	85.54	2
48	12.0	45	73.2	48.59	85.59	2
88	13.0	45	73.1	48.69	85.59	2
14	14.0	45	73.4	48.59	85.59	2
20	15.0	45	73.2	48.64	85.59	2
65	3.0	0	72.9	48.69	85.69	2
33	3.5	0	72.9	48.69	85.69	2
77	4.0	0	73.1	48.64	85.59	2
47	4.5	0	73.2	48.59	85.49	2
19	5.0	0	73.2	48.64	85.49	2

OBS	RADIUS	ANGLE	TEMP	TT1	TT2	PLATE
89	5.5	0	73.1	48.64	85.49	2
9	6.0	0	73.1	48.89	85.49	2
57	6.5	0	72.9	48.74	85.54	2
75	7.0	0	73.1	48.64	85.44	2
27	7.5	0	73.0	48.59	85.44	2
46	8.0	0	73.2	48.59	85.44	2
64	8.5	0	72.9	48.64	85.49	2
28	9.0	0	73.0	48.59	85.49	2
90	10.0	0	73.1	48.59	85.49	2
15	11.0	0	73.4	48.64	85.54	2
76	12.0	0	73.1	48.64	85.54	2
34	13.0	0	72.9	48.59	85.49	2
1	14.0	0	72.7	48.64	85.49	2
58	15.0	0	72.9	48.79	85.69	2

VITA

Paul Gerard Junghans was born on November 9, 1964 in Somerville, New Jersey He is the youngest of the four children of Mr. Philip and Teresa Junghans. He graduated from Strake Jesuit College Preparatory in 1983 In May of 1988, he completed his Bachelor of Science degree in Mechanical Engineering at Texas A&M University. Paul immediately entered the Masters of Science program in Mechanical Engineering at Texas A&M University and served as both a Research and Teaching Assistant. This thesis is submitted in partial fulfillment of the requirements for that degree. In June of 1990, Paul accepted permanent employment with Atlas Wireline Services in Houston, Texas His permanent phone number and address are (713)467-4913 and 13402 Alchester, Houston, Texas 77079-7104.